The IMD and JNK pathways drive the functional integration of the immune and circulatory systems of mosquitoes

Yan Yan [1#], Leah T. Sigle [1#], David C. Rinker [1], Tania Y. Estévez-Lao [1], John A. Capra [1,2] and Julián F. Hillyer [1*]

[1] Department of Biological Sciences, Vanderbilt University, Nashville, TN, USA

[2] Bakar Computational Health Sciences Institute and Department of Epidemiology and Biostatistics, University of California San Francisco. San Francisco, CA, USA

[#] Contributed equally

* Corresponding author: julian.hillyer@vanderbilt.edu

ORCID IDs (https://orcid.org/):

Yan Yan	0000-0002-4994-2651
Leah T. Sigle	0000-0003-2643-3587
David C. Rinker	0000-0001-5894-7633
Tania Y. Estévez-Lao	0000-0003-4671-8766
John A. Capra	0000-0001-9743-1795
Julián F. Hillyer	0000-0002-3178-0201

Abstract

The immune and circulatory systems of animals are functionally integrated. In mammals, the spleen and lymph nodes filter and destroy microbes circulating in the blood and lymph, respectively. In insects, immune cells that surround the heart valves (ostia), called periostial hemocytes, destroy pathogens in the areas of the body that experience the swiftest hemolymph (blood) flow. An infection recruits additional periostial hemocytes, amplifying heart-associated immune responses. Although the structural mechanics of periostial hemocyte aggregation have been defined, the genetic factors that regulate this process remain less understood. Here, we conducted RNAseq in the African malaria mosquito, *Anopheles gambiae*, and discovered that an infection upregulates multiple components of the IMD and JNK pathways in the heart with periostial hemocytes. This upregulation is greater in the heart with periostial hemocytes than in the circulating hemocytes or the entire abdomen. RNAi-based knockdown then showed that the IMD and JNK pathways drive periostial hemocyte aggregation and alter phagocytosis and melanization on the heart, thereby demonstrating that these pathways regulate the functional integration between the immune and circulatory systems. Understanding how insects fight infection lays the foundation for novel strategies that could protect beneficial insects and harm detrimental ones.

Keywords: Hemocytes; Heart; Insect; Melanization; Phagocytosis

38 **1. Introduction**

39 Insect immune cells, called hemocytes, produce pattern recognition receptors
40 that detect microbial invaders, activate immune signaling pathways, and kill pathogens
41 via phagocytosis, lysis, melanization and other mechanisms (1-3). These hemocytes
42 exist in a dynamic body cavity called the hemocoel, where the flow of hemolymph
43 constantly circulates them throughout the body. However, not all hemocytes circulate;
44 one quarter of hemocytes are attached to tissues and remain sessile (4). A sub-
45 population of these sessile hemocytes concentrates on the outer surface of the heart
46 and, more specifically, in the regions surrounding heart valves called ostia (5, 6). These
47 heart-associated hemocytes, called periostial hemocytes, reside in the locations of the
48 body that experience the highest hemolymph flow, and intensely phagocytose bacteria
49 and malaria parasites within seconds of their entry into the hemocoel. As this is
50 happening, additional hemocytes leave circulation and aggregate in the periostial
51 regions of the heart, thereby augmenting the heart-associated immune response (5, 6).
52 Although the kinetics and structural mechanics of periostial immunity have only been
53 described in the African malaria mosquito, *Anopheles gambiae* (5-9), heart-associated
54 immune responses have also been reported in other mosquito species, fruit flies, stick
55 insects, and moths (10-12). Further analysis of insects from 16 different orders showed
56 that the functional integration between the immune and circulatory systems is
57 conserved across the entire insect lineage (13).

58 In mosquitoes, pattern recognition receptors in the thioester-containing protein
59 family, together with adhesion and phagocytosis factors in the Nimrod protein family,
60 positively regulate immune responses on the heart (14, 15). However, heart-associated

61 immune responses are triggered by both bacterial and malarial infections, and by both
62 peptidoglycan and B-1,3-glucan (5, 6). Hence, the regulatory networks that drive
63 periostial hemocyte aggregation undoubtedly extend beyond pattern recognition
64 receptors and adhesion molecules. In insects, immune responses are primarily driven
65 by pathways such as Toll, immune deficiency (IMD), c-Jun N-terminal kinase (JNK), and
66 Jak/Stat (1, 16). The Toll pathway acts via the transcription factor Rel1, and primarily
67 responds to Gram(+) bacteria, fungi and rodent malaria parasites, whereas the IMD and
68 interlinked JNK pathways act via the transcription factors Rel2 and JNK, respectively,
69 and primarily respond to Gram(–) bacteria and human malaria parasites (17, 18). In fruit
70 flies, the Toll pathway is also involved in hemocyte differentiation, and its constitutive
71 activation disrupts sessile hemocytes (19, 20). The IMD pathway has not been directly
72 linked to cellular immunity but its canonical activator, the peptidoglycan recognition
73 protein PGRP-LC, positively regulates phagocytosis of *Escherichia coli* but not
74 *Staphylococcus aureus* (21). The Jak/Stat pathway acts via the Stat family of
75 transcription factors. In mosquitoes, this pathway responds to malaria parasites and
76 viruses (22, 23), and in fruit flies it controls hemocyte maturation and differentiation (24,
77 25).

78 The goal of this study was to identify genes and regulatory pathways that drive
79 periostial hemocyte aggregation in *A. gambiae*. Using an unbiased RNA sequencing
80 (RNAseq) approach that was followed by empirical testing with RNA interference
81 (RNAi), we uncovered that the IMD and JNK pathways drive periostial hemocyte
82 aggregation and immune responses on the heart, thereby regulating the functional
83 integration between the immune and circulatory systems of mosquitoes.

84

85 **2. Results**

86 *2.1. Infection upregulates immune genes in periostial hemocytes*

87 To identify genes that may drive periostial hemocyte aggregation, we undertook
88 an unbiased RNAseq approach where we sequenced the transcriptome of tissues from
89 mosquitoes that were naïve, injured, or infected with Gram(–) GFP-*E. coli* or Gram(+) *S.*
90 *aureus* (Figure 1A-B; *Dataset* S1). Three tissues were isolated at 4 hr after treatment: (i)
91 the heart containing periostial hemocytes, (ii) the hemolymph containing circulating
92 hemocytes, and (iii) the entire abdomen. Mosquitoes were assayed at 4 hr after
93 treatment because the number of periostial hemocytes approximately doubles within the
94 first hour of infection, and plateaus by 4 hr after infection (5). In these experiments, most
95 mosquitoes were used for sequencing, but a subset of mosquitoes was used to confirm
96 that infection induces heart-associated cellular immune responses. Indeed, a resident
97 population of periostial hemocytes was present in both naïve and injured mosquitoes,
98 and the number of periostial hemocytes increased 1.8- and 1.6-fold after GFP-*E. coli*
99 and *S. aureus* infection, respectively (Figure 1B-C).

100 RNAseq revealed that, relative to the heart and periostial hemocytes of naïve
101 and injured mosquitoes, 73 and 132 genes are upregulated more than 4-fold ($P < 0.05$)
102 in the heart and periostial hemocytes of mosquitoes infected with GFP-*E. coli* and *S.*
103 *aureus*, respectively (Figure 1D). Because periostial hemocyte aggregation is a dynamic
104 immune response that occurs during any bacterial infection, we hypothesized that its
105 core molecular drivers must be preferentially upregulated in periostial hemocytes
106 following both *E. coli* and *S. aureus* infection. We found that 55 genes met this overlap

107 criterion (Figure 1E; Table S1). Comparing the heart and periostial hemocyte RNAseq
108 data to RNAseq data from (i) circulating hemocytes and (ii) the entire abdomen then
109 revealed that infection upregulates more genes in the heart with periostial hemocytes
110 than in the circulating hemocytes or the abdomen (Figure 1D-E; Tables S1-S3).

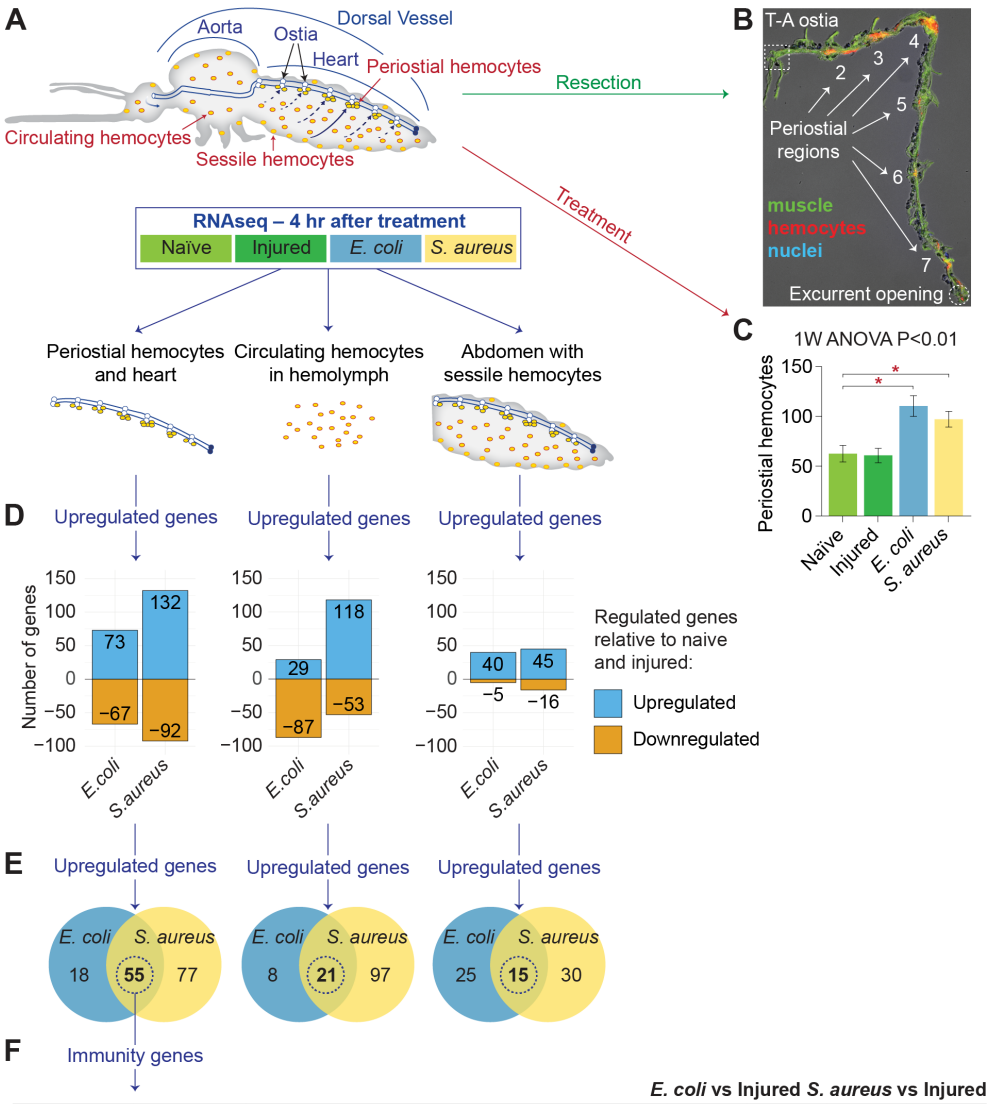

			E. coli vs Injured		*S. aureus* vs Injured	
Gene ID	**Gene name**	**Gene description**	**log2FC**	**P value**	**log2FC**	**P value**
AGAP000694	***cec3***	cecropin anti-microbial peptide	2.72	8E-14	3.20	2E-19
AGAP001212	*PGRPLB*	peptidoglycan recognition protein (long)	3.10	2E-25	4.21	3E-47
AGAP001648	*CLIPB17*	CLIP-domain serine protease	2.24	4E-10	3.01	3E-18
AGAP005205	***PGRPLA***	peptidoglycan recognition protein (long)	2.36	7E-47	2.66	1E-60
AGAP006747	***rel2***	NF-kappaB Relish-like transcription factor	2.00	2E-33	2.21	3E-41
AGAP009091	*ddc*	dopa decarboxylase	3.96	2E-50	4.81	3E-75
AGAP009213	*SRPN16*	serine protease inhibitor (serpin) 16	2.61	8E-13	3.75	1E-26
AGAP009214	*CLIPB11*	CLIP-domain serine protease	2.13	1E-06	3.71	2E-19
AGAP009460	***JNK3***	c-Jun N-terminal kinase	2.22	1E-04	3.47	1E-10
AGAP011294	***def1***	defensin anti-microbial peptide	2.13	2E-05	2.70	1E-08
AGAP011326	***IAP2***	inhibitor of apoptosis 2	3.21	2E-38	3.29	1E-40
AGAP013506	*upd3a*	JAK/STAT pathway cytokine unpaired 3 variant A	3.89	2E-12	4.05	8E-14

111
112

113 **Figure 1. Infection upregulates immune genes in periostial hemocytes.** (*A*) The
114 heart with periostial hemocytes, the circulating hemocytes, and the abdomen of
115 mosquitoes that were naïve, injured, or infected with GFP-*E. coli* or *S. aureus* were
116 sequenced by RNAseq at 4 hr post-treatment. (*B*) Fluorescence and DIC overlay shows
117 that the periostial hemocytes (red) remain attached to a resected heart (green). Marked
118 are the periostial regions for each abdominal segment, the thoraco-abdominal (T-A)
119 ostia and the posterior excurrent opening. Image is modified from Sigle and Hillyer (7),
120 and reproduced according to Creative Commons Attribution License CC BY. (*C*) Naïve
121 and injured mosquitoes have resident periostial hemocytes, but infection for 4 hr with
122 GFP-*E. coli* or *S. aureus* induces the aggregation of additional hemocytes at the
123 periostial regions. Whiskers show the standard error of the mean (S.E.M.; n = 14 for all
124 groups). (*D*) Bar plots show the number of genes significantly upregulated or
125 downregulated at 4 hr after GFP-*E. coli* or *S. aureus* infection in the periostial
126 hemocytes and heart (left), the circulating hemocytes (middle), and the entire abdomen
127 (right). (*E*) Venn diagrams show that 55, 21 and 15 genes are significantly upregulated
128 in the periostial hemocytes, the circulating hemocytes or the abdomen, respectively,
129 during both GFP-*E. coli* and *S. aureus* infections. (F) Table listing the immune genes
130 that are among the 55 genes that were upregulated in the heart with periostial
131 hemocytes following both GFP-*E. coli* or *S. aureus* infection. Genes that participate in
132 the IMD and JNK pathway are in bold.
133

134 We then scrutinized the reported function of the 55 candidate genes. Twelve
135 have immune function (Figure 1F), and strikingly, 6 are part of IMD and JNK pathway:
136 the peptidoglycan recognition protein *PGRP-LA* (26), the inhibitor of apoptosis family
137 member *IAP2* (27), the IMD pathway transcription factor *rel2* (28, 29), the antimicrobial
138 peptides *cec3* (29) and *def1* (30, 31), and the JNK pathway transcription factor *JNK3*
139 (32, 33). Multiple aspects of the IMD and JNK pathway are represented: upstream
140 components such as *PGRP-LA* and *IAP2*, and downstream elements from both
141 branches of the pathway, with the classical IMD cascade represented by *rel2*, *cec3* and
142 *def1*, and the bifurcation into the JNK pathway represented by *JNK3* (27, 34, 35) (Figure
143 S1). Relevant to this finding, activating the IMD pathway induces the expression of the
144 scavenger and phagocytosis receptor *eater* (36), which positively regulates hemocyte
145 adhesion in fruit flies and periostial hemocyte aggregation in mosquitoes (15, 37). The

146 IMD pathway also induces the expression of the thioester containing protein *TEP1*,
147 which is involved in phagocytosis and periostial hemocyte aggregation (14). Moreover,
148 transglutaminases are pleiotropic enzymes that in *Drosophila* inhibit the IMD pathway
149 (38, 39), and a mosquito transglutaminase – *TGase3* – negatively regulates periostial
150 hemocyte aggregation and has infection-dependent effects on the heart rate (40, 41).
151 Finally, the JNK pathway is associated with cell adhesion and phagocytosis by
152 regulating the cytoskeleton (32, 42). The JNK pathway also induces the expression of
153 the engulfment receptor *draper* (43) and *TEP1* (33), both of which affect periostial
154 hemocyte aggregation in mosquitoes (14, 15). All six IMD and JNK pathway genes
155 identified in our unbiased screen were more highly upregulated in the heart and
156 periostial hemocytes than in the other tissues (Figure S2). The remaining six candidate
157 genes with immune function that were identified in our screen – *CLIPB17*, *DDC*,
158 *SRPN16*, *CLIPB11*, *PGRP-LB* and *upd3k* – do not participate in a common pathway.
159 Because the downregulation of genes could also impact hemocyte aggregation,
160 we assessed the genes that were downregulated after both *E. coli* and *S. aureus*
161 infection, relative to naïve and injured mosquitoes. No genes met this criterion for the
162 abdomen, but 29 genes met this criterion for the heart with periostial hemocytes and 19
163 genes for the circulating hemocytes (Tables S4 and S5). Five of these genes were
164 shared between the heart with periostial hemocytes and the circulating hemocytes, but
165 none of the 43 genes have a classical role in immunity or carry a function suggestive of
166 involvement in hemocyte aggregation. Therefore, based on the RNAseq analyses we
167 hypothesized that the main driver of periostial hemocyte aggregation is the IMD and
168 JNK pathway.

169

170 *2.2. The IMD pathway positively regulates periostial hemocyte aggregation*

171 To determine whether the IMD pathway regulates periostial hemocyte
172 aggregation, we synthesized double-stranded RNA (dsRNA) to target the IMD cascade
173 transcription factor, *rel2*, and its negative regulator, *caspar*, and achieved RNAi-based
174 silencing of 43% and 37%, respectively, compared to the ds*bla(Ap^R)* control mosquitoes
175 (Figure S3). Moreover, because *Tep1* is (i) activated by the Rel2 arm of the IMD
176 pathway (44, 45) and (ii) a positive driver of periostial hemocyte aggregation (14), we
177 measured its mRNA abundance in *rel2* and *caspar* RNAi mosquitoes. Silencing of *rel2*
178 did not alter *TEP1* mRNA abundance but silencing of *caspar* increased it. Because *cec3*
179 and *def1* are also activated by Rel2 (29-31), we measured their mRNA abundance in
180 RNAi mosquitoes. Silencing of *rel2* decreased *cec3* and *def1* mRNA abundance
181 whereas silencing of *caspar* increased them (Figure S3). Overall, these data are
182 consistent with the role that the Rel2 arm of the IMD pathway plays in regulating *TEP1*,
183 *cec3* and *def1* expression.

184 To assess whether the IMD pathway drives heart-associated immune responses,
185 we compared the number and activity of periostial hemocytes in *rel2* and *caspar* RNAi
186 mosquitoes, relative to ds*bla(Ap^R)* control mosquitoes (Figure 2 and 3). As expected,
187 infection for 4 hr induced the aggregation of hemocytes at the periostial regions of
188 ds*bla(Ap^R)* mosquitoes, and this aggregation remained in place at 24 hr. In uninfected
189 mosquitoes, knocking down *rel2* did not change the number of periostial hemocytes, but
190 at 4 hr following infection, knockdown of *rel2* decreased the number of periostial
191 hemocytes by 18%, relative to ds*bla(Ap^R)* mosquitoes (Figure 2A-B). At 24 hr post-

192 infection, the effect of *rel2* RNAi on periostial hemocyte aggregation was diminished.
193 When we instead knocked down *caspar*, the number of periostial hemocytes increased
194 by 39% in uninfected mosquitoes, and infection for 4 and 24 hr increased the number of
195 periostial hemocytes by 30% and 19%, respectively, relative to similarly treated
196 ds*bla(Ap^R)* mosquitoes. This shows that *rel2* positively regulates periostial hemocyte
197 aggregation whereas *caspar* negatively regulates this process.
198 To determine whether the IMD pathway specifically affects periostial hemocytes
199 and not sessile hemocytes in general, we counted the number of sessile hemocytes
200 outside of the periostial regions in the tergum of abdominal segments 4 and 5 in the
201 same mosquitoes examined for periostial hemocytes (Figure 2C). Knockdown of *rel2* or
202 *caspar* did not alter the number of non-periostial sessile hemocytes in uninfected
203 mosquitoes or mosquitoes infected for 4 hr. However, at 24 hr following infection,
204 *caspar* RNAi decreased non-periostial sessile hemocytes by 22%. These results
205 demonstrate that the IMD pathway regulates periostial hemocyte aggregation while
206 having a minimal effect on the rest of the sessile hemocytes.

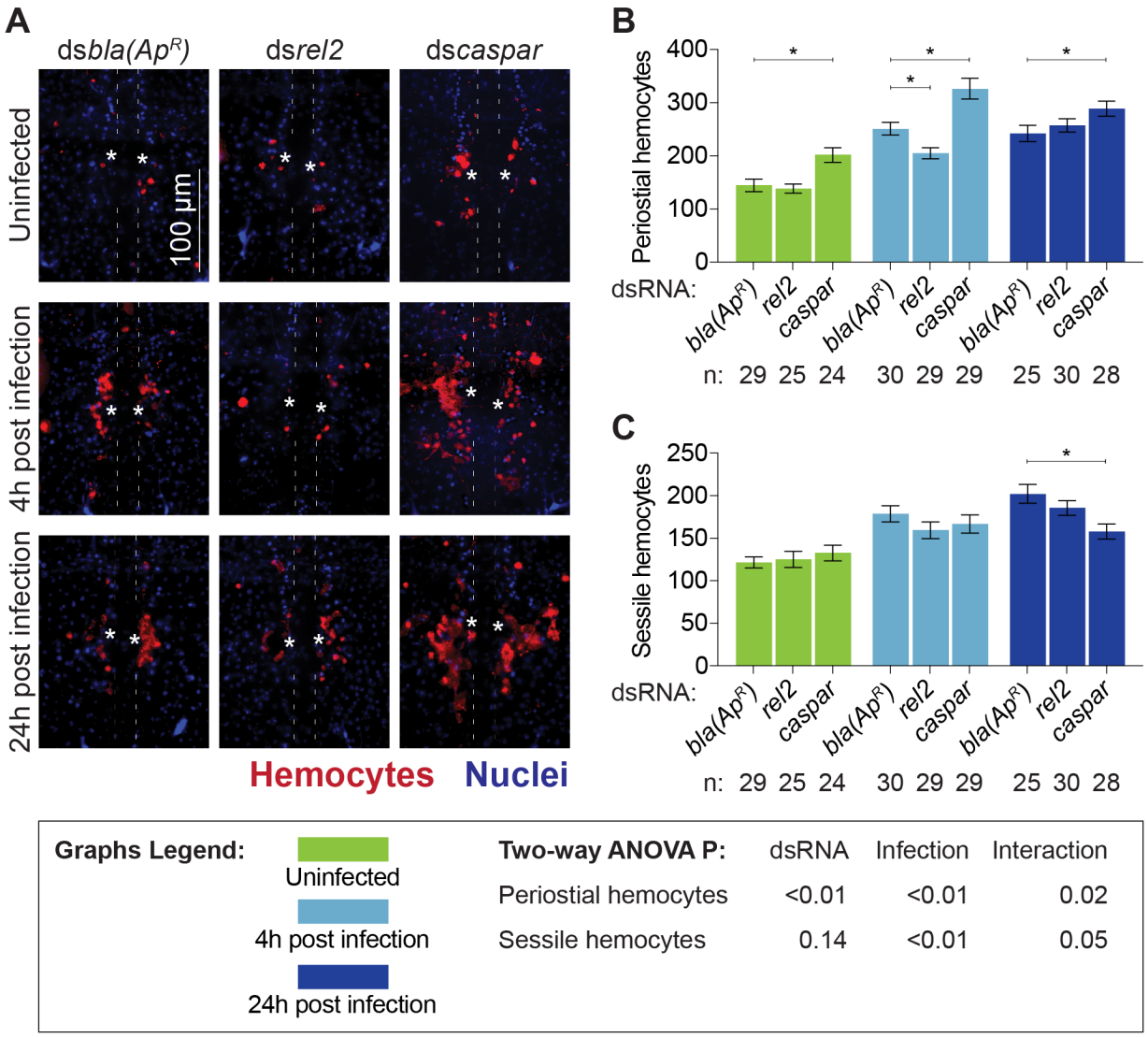

Figure 2. The IMD pathway drives periostial hemocyte aggregation. (*A*) Fluorescence images show periostial hemocytes (CM-DiI; red) surrounding a single pair of ostia (asterisks) on a segment of the heart (outlined by dotted lines) of ds*bla(Ap^R)*, ds*rel2* and ds*caspar* mosquitoes that were not infected or had been infected with GFP-*E. coli* for 4 or 24 hr. Anterior is on top. (*B-C*) Graphs for ds*bla(Ap^R)*, ds*rel2* and ds*caspar* mosquitoes that were not infected or had been infected with GFP-*E. coli* for 4 or 24 hr. The graphs show: (*B*) average number of periostial hemocytes; and (*C*) average number of sessile hemocytes outside of the periostial regions in the tergum of abdominal segments 4 and 5. Graphs show the mean and S.E.M. The data were analyzed by two-way ANOVA (bottom box), followed by Dunnett's multiple comparison test. N indicates sample size. Asterisks in graphs indicate post-hoc $P < 0.05$.

221 Periostial hemocytes phagocytose bacteria, leading to their accumulation at the
222 periostial regions (5, 6). To determine whether the IMD pathway affects the phagocytic
223 activity of periostial hemocytes, we measured the GFP-*E. coli* fluorescence pixel area in
224 the periostial regions of infected mosquitoes (Figure 3A; Figure S4). At 4 hr following
225 infection, the GFP-*E. coli* pixel area was similar regardless of dsRNA treatment. At 24 hr
226 after infection, this area decreased in ds*bla(Ap^R)* and ds*caspar* mosquitoes, indicating
227 that periostial hemocytes efficiently destroyed the pathogens. However, at 24 hr
228 following infection, *rel2* RNAi significantly increased GFP-*E. coli* accumulation at the
229 periostial regions. Periostial hemocytes also phagocytose melanized bacteria (5, 6), and
230 one melanization related-gene – dopa decarboxylase or *DDC* (46, 47) – was
231 upregulated in both the heart with periostial hemocytes and the circulating hemocytes.
232 Therefore, we measured melanin accumulation in the periostial regions (Figure 3B;
233 Figure S4). Melanin was absent in uninfected mosquitoes and mosquitoes that were
234 infected for 4 hr. However, at 24 hr following infection, *rel2* RNAi increased melanin
235 deposits at the periostial regions whereas *caspar* RNAi had no effect.

236 The increased accumulation of GFP-*E. coli* and melanin in *rel2* RNAi mosquitoes
237 at 24 hr after infection could be due to either (i) enhanced phagocytosis by periostial
238 hemocytes, or (ii) higher bacterial proliferation in the hemocoel, which places increased
239 pressure on the phagocytosis response. To differentiate between these two scenarios,
240 we measured the systemic GFP-*E. coli* infection intensity and observed that, at 4 hr after
241 infection, the bacterial intensity was similar for all dsRNA treatments, but at 24 hr,
242 knockdown of *rel2* resulted in a higher infection intensity than treatment with ds*caspar* or
243 ds*bla(Ap^R)* (Figure 3C). This suggests that *rel2* is essential for proper bacterial killing in

244 the hemocoel, and therefore, knocking it down increases infection intensity in a manner
245 that leads to increased phagocytosis in the periostial regions. However, because silencing
246 *rel2* and *caspar* had opposite effects on periostial hemocyte aggregation at 4 hr, a time
247 when dsRNA treatment does not impact infection intensity, we conclude that the IMD
248 pathway is a positive regulator of periostial hemocyte aggregation.

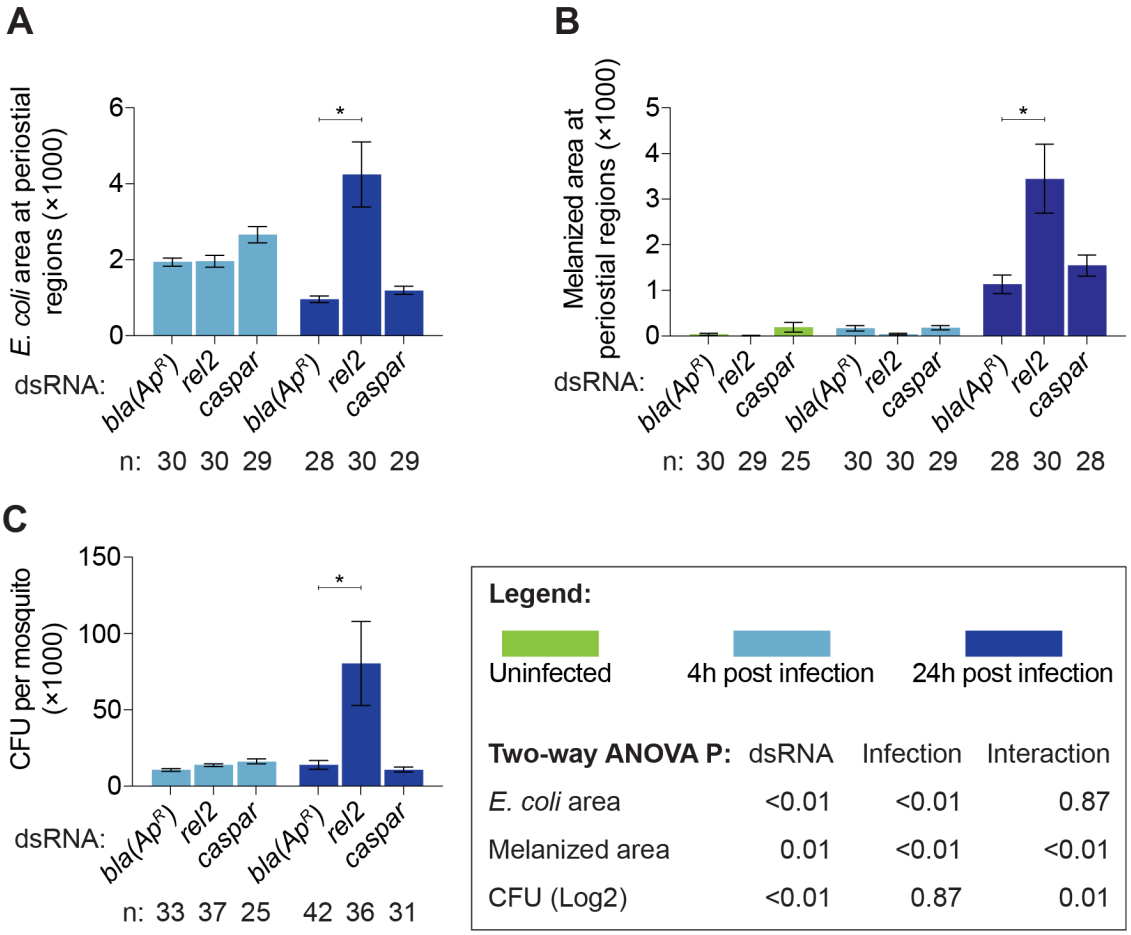

249

250 **Figure 3. The IMD pathway modulates immune responses on the heart and the**
251 **systemic antimicrobial response.** (*A*-*C*) Graphs for ds*bla(Ap^R)*, ds*rel2* and ds*caspar*
252 mosquitoes that were not infected or had been infected with GFP-*E. coli* for 4 or 24 hr.
253 The graphs show: (*A*) pixel area of GFP-*E. coli* in the periostial regions; (*B*) pixel area of
254 melanin in the periostial regions; and (*C*) the systemic GFP-*E. coli* infection intensity.
255 Graphs show the mean and S.E.M. The data were analyzed by two-way ANOVA
256 (bottom box), followed by Dunnett's multiple comparison test. N indicates sample size.
257 Asterisks in graphs indicate post-hoc $P < 0.05$.

258 PGRP-LC is the canonical activator of the IMD pathway (1), but PRGP-LA (i)
259 activates the IMD pathway in the midgut of mosquitoes and in the barrier epithelia of
260 fruit flies (26, 48), (ii) is expressed in *Drosophila* hemocytes (49), and (iii) is upregulated
261 in the heart and periostial hemocytes (Figure 1F). Therefore, we tested the involvement
262 of PGRP-LA in periostial hemocyte aggregation. *PGRP-LA* has three splice forms, so to
263 knock it down, we synthesized ds*PGRP-LA-RARB* to target the *RA* and *RB* splice
264 forms, and ds*PGRP-LA-RC* to target the *RC* splice form. Using these dsRNAs, we
265 achieved RNAi-based silencing that ranged from 56% to 77%, compared to the
266 ds*bla(Ap^R)* control mosquitoes (Figure S5). *PGRP-LA* knockdown with any dsRNA did
267 not alter the number of periostial hemocytes, the number of non-periostial sessile
268 hemocytes, melanin accumulation at the periostial regions, or systemic infection
269 intensity (Figure S6). However, knockdown of *PGRP-LA-RC* increased phagocytosis of
270 GFP-*E. coli* in the periostial regions, which suggests that the RC splice form is involved
271 in the phagocytosis response.
272

273 *2.3. The JNK pathway positively regulates periostial hemocyte aggregation*

274 We next tested whether the JNK pathway regulates periostial hemocyte
275 aggregation. *A. gambiae* encodes two JNK genes: *JNK1* and *JNK3* (50). Therefore, we
276 synthesized double-stranded RNA (dsRNA) to target the JNK cascade transcription
277 factors, *JNK1* and *JNK3*, and their negative regulator, *puckered* (*puc*). Because of high
278 sequence identity between *JNK1* and *JNK3*, ds*JNK1/3* simultaneously targeted both
279 JNK genes. RNAi-based knockdown resulted in 33%, 44% and 31% reduction in mRNA
280 abundance of *JNK1*, *JNK3* and *puc*, respectively (Figure S7). Moreover, because the

281 JNK pathway has also been implicated in the expression of *TEP1* (51), we measured
282 the mRNA abundance of *TEP1*, *cec3* and *def1* in *JNK1*/*JNK3* and *puc* RNAi
283 mosquitoes. Manipulating the JNK pathway did not have a clear impact on effector gene
284 expression (Figure S7). The lack of clarity on how the JNK pathway controls the
285 expression of *TEP1*, *cec3* or *def1* could be due to their co-regulation by other pathways,
286 or a consequence of incomplete gene silencing of *JNK1/3* and *puc*.
287 To assess whether the JNK pathway drives heart-associated immune responses,
288 we compared the number and activity of periostial hemocytes in *JNK1/3* and *puc* RNAi
289 mosquitoes, relative to ds*bla(Ap^R)* control mosquitoes (Figure 4 and 5). Regardless of
290 infection status, the number of periostial hemocytes was statistically similar between
291 ds*JNK1/3* and ds*bla(Ap^R)* mosquitoes, although ds*JNK1/3* mosquitoes averaged fewer
292 periostial hemocytes than control mosquitoes for all treatments (Figure 4A-B).
293 Knockdown of *puc*, however, increased the number of periostial hemocytes 1.6-fold in
294 uninfected mosquitoes, and 1.4- and 1.5-fold at 4 and 24 hr following GFP-*E. coli*
295 infection, respectively, relative to similarly treated ds*bla(Ap^R)* mosquitoes. To further
296 determine whether *puc* specifically affects periostial hemocytes or sessile hemocytes in
297 general, we quantified the number of non-periostial sessile hemocytes on the tergum of
298 the same mosquitoes (Figure 4C). *JNK1/3* RNAi mosquitoes showed a trend of fewer
299 non-periostial sessile hemocytes than control mosquitoes regardless of infection status.
300 Treatment with ds*puc*, however, increased the number of non-periostial sessile
301 hemocytes for all treatments. This demonstrates that the JNK pathway positively
302 regulates both periostial and non-periostial sessile hemocyte abundance.

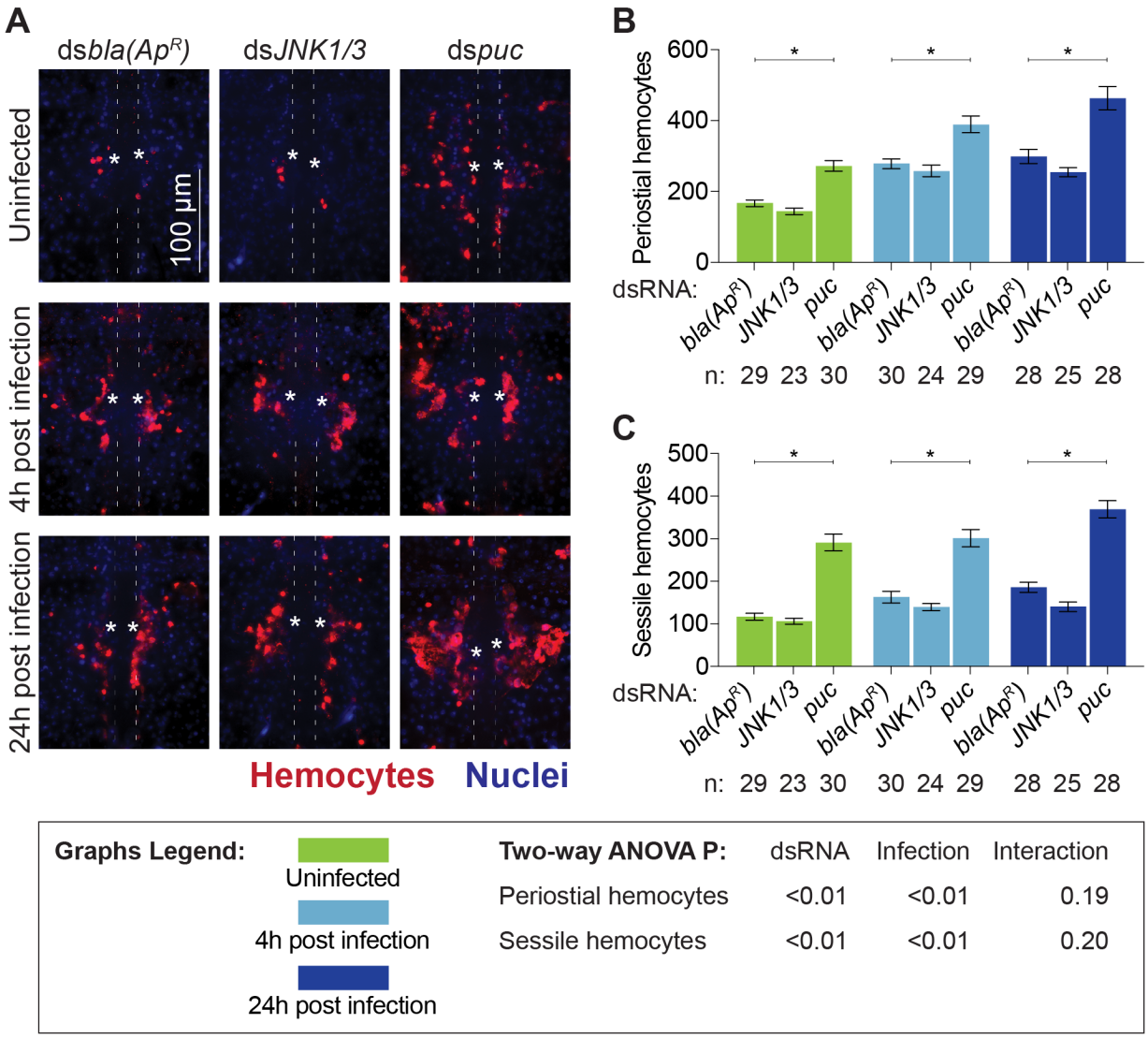

Figure 4. The JNK pathway drives periostial hemocyte aggregation. (*A*) Fluorescence images show periostial hemocytes (CM-DiI; red) surrounding a single pair of ostia (asterisks) on a segment of the heart (outlined by dotted lines) of ds*bla(Ap^R)*, ds*JNK1/3* and ds*puc* mosquitoes that were not infected or had been infected with GFP-*E. coli* for 4 or 24 hr. Anterior is on top. (*B*-*C*) Graphs for ds*bla(Ap^R)*, ds*JNK1/3* and ds*puc* mosquitoes that were not infected or had been infected with GFP-*E. coli* for 4 or 24 hr. The graphs show: (*B*) average number of periostial hemocytes; and (*C*) average number of sessile hemocytes outside of the periostial regions in the tergum of abdominal segments 4 and 5. Graphs show the mean and S.E.M. The data were analyzed by two-way ANOVA (bottom box), followed by Dunnett's multiple comparison test. N indicates sample size. Asterisks in graphs indicate post-hoc $P < 0.05$.

We next measured whether the JNK pathway affects the phagocytic activity of periostial hemocytes (Figure 5A; Figure S8). At 4 hr following infection, the GFP-*E. coli*

318 pixel area was similar regardless of dsRNA treatment. However, at 24 hr following
319 infection, periostial hemocytes in ds*puc* mosquitoes phagocytosed more GFP-*E. coli*
320 than the ds*bla(Ap^R)* mosquitoes. We then quantified the melanized bacteria that were
321 sequestered by periostial hemocytes (Figure 5B; Figure S8). Melanin deposits were
322 undetectable in uninfected mosquitoes and mosquitoes at 4 hr post infection; however,
323 at 24 hr following GFP-*E. coli* infection, more melanin was present in ds*puc* mosquitoes
324 than in ds*bla(Ap^R)* controls.

325

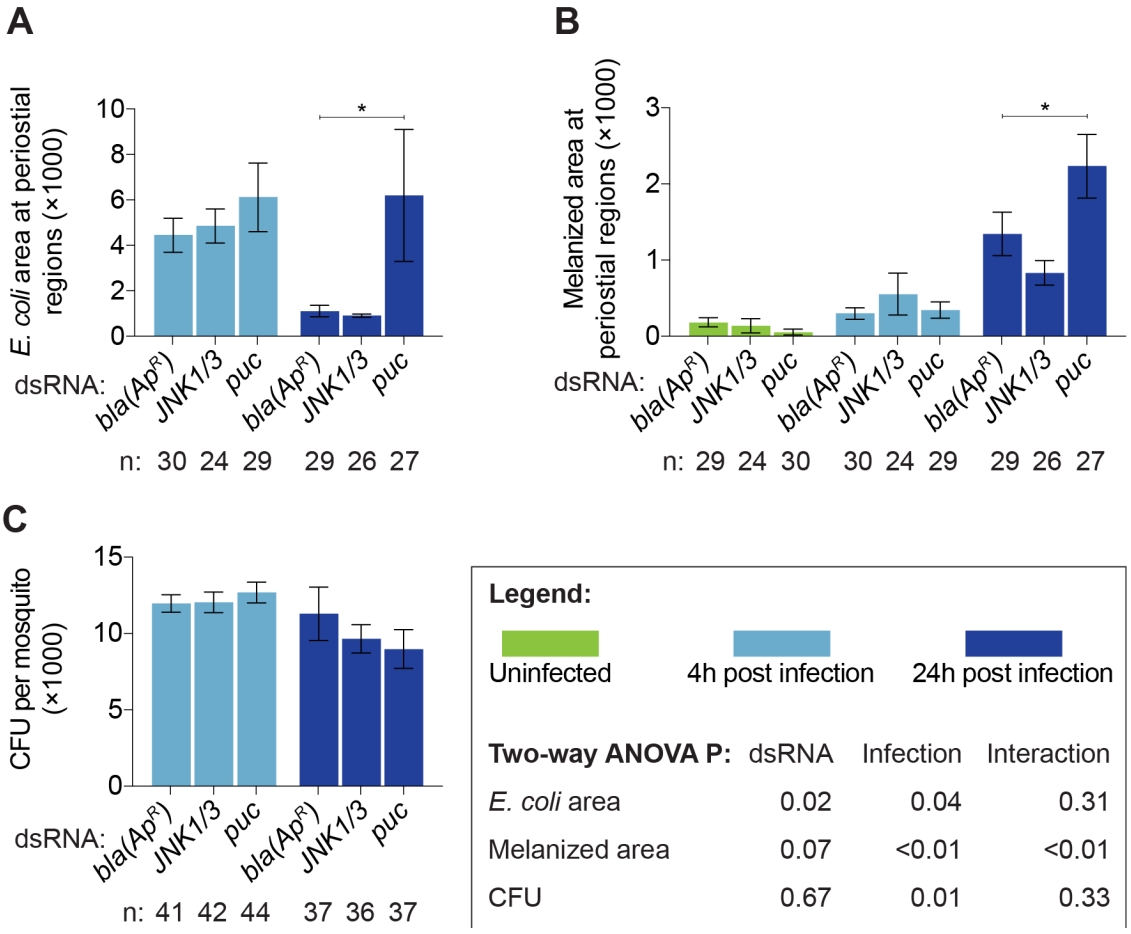

Two-way ANOVA P:	dsRNA	Infection	Interaction
E. coli area	0.02	0.04	0.31
Melanized area	0.07	<0.01	<0.01
CFU	0.67	0.01	0.33

326
327
328
329 **Figure 5. The JNK pathway modulates immune responses on the heart but not the**
330 **systemic antimicrobial response.** (*A*-*C*) Graphs for ds*bla(Ap^R)*, ds*JNK1/3* and ds*puc*
331 mosquitoes that were not infected or had been infected with GFP-*E. coli* for 4 or 24 hr.
332 The graphs show: (*A*) pixel area of GFP-*E. coli* in the periostial regions; (*B*) pixel area of

333 melanin in the periostial regions; and (*C*) the systemic GFP-*E. coli* infection intensity.
334 Graphs show the mean and S.E.M. The data were analyzed by two-way ANOVA
335 (bottom box), followed by Dunnett's multiple comparison test. N indicates sample size.
336 Asterisks in graphs indicate post-hoc $P < 0.05$.
337

338 The difference in GFP-*E. coli* and melanin accumulation in ds*puc* mosquitoes
339 could be due to (i) enhanced phagocytosis by periostial hemocytes, or (ii) higher
340 bacterial proliferation in the hemocoel. To differentiate between these two scenarios, we
341 quantified the systemic *E. coli* infection intensity and found that the bacterial intensity
342 was similar regardless of dsRNA treatment (Figure 5C). Therefore, this suggests that
343 *puc* negatively regulates hemocyte adhesion and phagocytic activity, and demonstrates
344 that the JNK pathway is a positive regulator of periostial immune responses.
345

346 **3. Discussion**

347 Previous microarray and RNAseq analyses revealed genes and signaling
348 pathways that are active in hemocytes (52-58), including those that are activated in
349 specific subpopulations of hemocytes (59-61). However, these studies only focused on
350 circulating hemocytes, and therefore, failed to capture the biology of sessile hemocytes.
351 Yet, one quarter of hemocytes are sessile (4), and they play significant roles in
352 hematopoiesis (62, 63), wound healing (64), and pathogen killing (9, 65, 66). Therefore,
353 extrapolating the molecular signatures of circulating hemocytes to those of sessile
354 hemocytes likely misses the essential factors that make sessile hemocytes conduct
355 their specific immune activities. Periostial hemocytes are a subpopulation of sessile
356 hemocytes that reside on the heart, where they sequester and kill pathogens in areas of
357 high hemolymph flow (5, 6, 13). To better understand how an infection drives the

358 migration of hemocytes to the heart and how these immune cells kill pathogens at the
359 periostial regions, we sequenced the periostial hemocyte transcriptome and discovered
360 that the IMD and JNK pathway drives periostial immune responses (Figure 6).

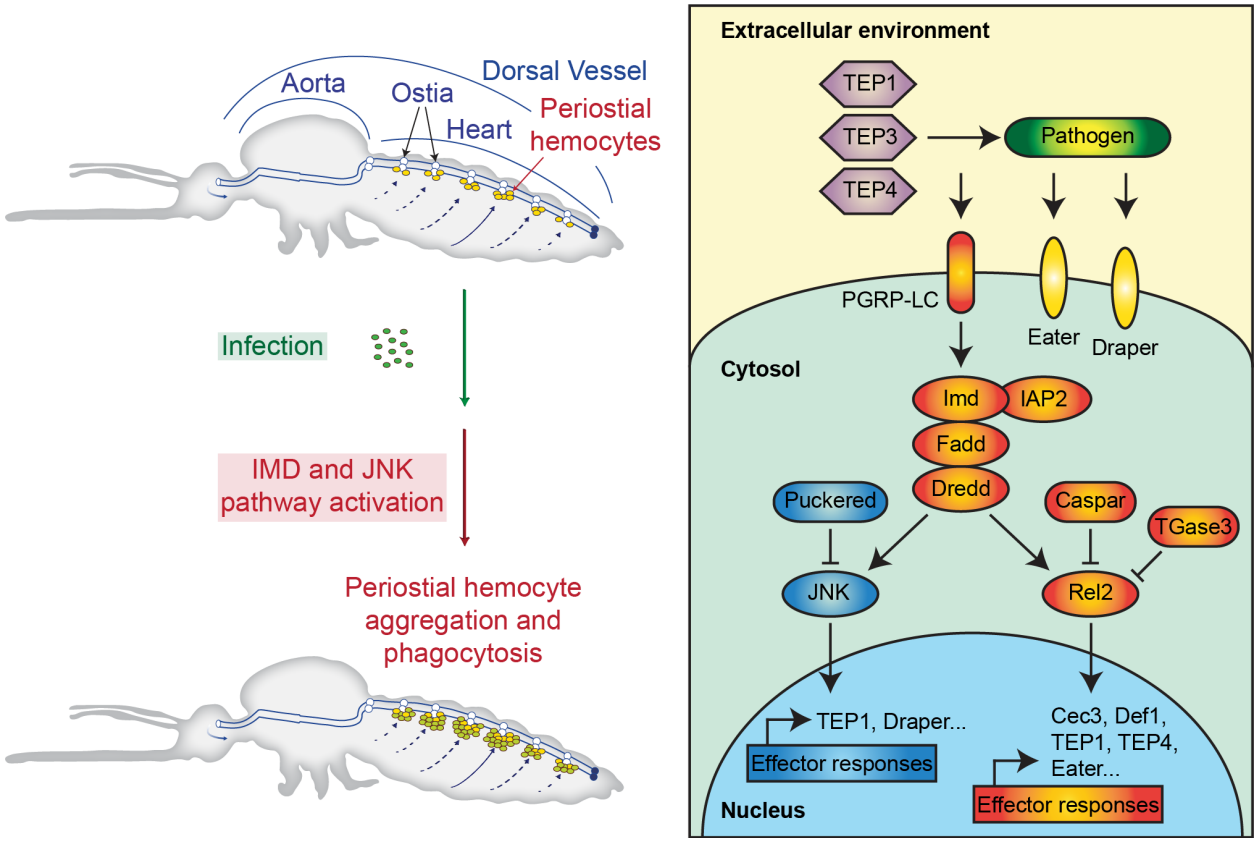

361
362
363 **Figure 6. The IMD and JNK pathways, together with TEP proteins (TEP1, TEP3**
364 **and TEP4), Nimrod proteins (Draper and Eater) and a transglutaminase, regulate**
365 **heart-associated immune responses in mosquitoes.**
366

367 The IMD pathway controls the production of antimicrobial peptides (1, 27), but
368 here we show that the IMD pathway also regulates a cellular immune response: the
369 transition of hemocytes from a circulating to a sessile state on the heart. Specifically,
370 knockdown of the positive regulator of the IMD pathway, *rel2*, decreases infection-
371 induced periostial hemocyte aggregation, whereas knockdown of the negative regulator
372 of the IMD pathway, *caspar*, increases the number of periostial hemocytes. We

373 hypothesize that the IMD pathway drives periostial hemocyte aggregation via two
374 cascades that are also driving phagocytosis: the TEP1-TEP3-LRP1-CED6L and TEP4-
375 BINT2-CED2L-CED5L pathways (67). The IMD pathway induces the expression of
376 *TEP1* and *TEP4* (30, 31, 68), and both of these genes positively regulate periostial
377 hemocyte aggregation (14). Moreover, two downstream molecules – the low-density-
378 lipoprotein-receptor-related protein LRP1 and the beta integrin BINT2 – are
379 transmembrane proteins that in mammals and insects have overlapping functions in
380 phagocytosis and adhesion (69-71), and therefore, likely facilitate the adhesion of
381 hemocytes to the heart. In this study, we also confirmed the positive role that REL2
382 plays in pathogen killing (29, 44, 68, 72-78). When we systemically knocked down the
383 expression of *rel2*, bacteria proliferated uncontrollably during the later stages of
384 infection. We hypothesize that knocking down *rel2* initially suppresses periostial
385 hemocyte aggregation, but as the infection progresses and the intensity increases, the
386 necessity of periostial immune responses also increases, and this pressure recruits
387 hemocytes to the heart and enhances their collective phagocytic activity. Overall, our
388 data show that the IMD pathway drives periostial hemocyte aggregation during the early
389 stages of infection and limits systemic infection intensity during the later stages of
390 infection.

391 The JNK pathway modulates mosquito longevity, regulates oviposition, and limits
392 infection with malaria parasites and viruses (33, 51, 79-82). Here, we found that
393 overexpressing the JNK pathway by knocking down the negative regulator, *puc*,
394 increases the number of periostial and adjacent sessile hemocytes. This suggests that
395 the JNK pathway positively regulates hemocyte adhesion. Indeed, the *Drosophila*

396 ortholog of mosquito *JNK1* and *JNK3*, called *basket*, is involved in the formation of
397 actin-rich and focal adhesion kinase-rich placodes in hemocytes (83). The JNK pathway
398 also induces hemocyte differentiation in *Drosophila*, producing large lamellocytes that
399 adhere and encapsulate parasitoid eggs (84). We found that overactivating the JNK
400 pathway does not alter infection intensity in mosquitoes, but it increases the
401 accumulation of *E. coli* and melanin on the heart, suggesting that the JNK pathway
402 positively regulates the phagocytosis and melanization responses. Indeed, JNK1
403 positively regulates melanization in mosquitoes that are refractory to malaria (51), and
404 overexpressing the JNK pathway in aphids increases the melanin-producing activity of
405 phenoloxidase and the phagocytic activity of hemocytes (85). We hypothesize that the
406 JNK pathway regulates phagocytosis by periostial hemocytes in a manner that involves
407 two proteins already known to be involved in periostial hemocyte aggregation: TEP1
408 and draper (14, 15). The JNK pathway activates the expression of both of these genes
409 (33, 80, 86), and TEP1 opsonizes pathogens for phagocytosis whereas draper activates
410 phagocytic processes (14, 15, 67, 87-89). In our study, we could not distinguish
411 between the roles that *JNK1* and *JNK3* play in periostial hemocyte aggregation.
412 However, simultaneous knockdown of both resulted in phenotypes that were opposite of
413 *puc* knockdown, strongly suggesting that JNK1 or JNK3 – or both – positively regulates
414 periostial hemocyte aggregation.
415 Because both the IMD and JNK pathways induce the production of *TEP1* (30, 33,
416 68, 80), we hypothesize that they share the TEP1-TEP3-LRP1-CED6L phagocytosis
417 cascade that leads to hemocyte aggregation. However, we also hypothesize that the
418 IMD and JNK pathways use additional, independent mechanisms to regulate periostial

419 hemocyte aggregation for three reasons. First, even though the two pathways share
420 upstream signaling molecules, they bifurcate and activate their own set of effector
421 genes (34, 35). Second, knocking down the components of the IMD and JNK pathways
422 resulted in different phenotypes, especially for periostial and non-periostial sessile
423 hemocytes. Third, in *Drosophila*, draper and the BINT2 ortholog (Integrin βν) function
424 independently (90), and in mosquitoes, draper is regulated by the JNK pathway
425 whereas BINT2 is involved in the IMD-regulated and TEP4-mediated phagocytosis
426 cascade (31, 67, 70, 86).

427 Bacteria, malaria parasites, and fungal components all induce periostial
428 hemocyte aggregation, and this process is structurally conserved across the entire
429 insect lineage (5, 6, 13). Therefore, it is likely that other proteins contribute to this
430 process. Indeed, infection also induces the upregulation of *Upd3* by periostial
431 hemocytes, which is a ligand for the receptor of the JAK/STAT pathway (91). The TOLL
432 pathway also induces hemocyte proliferation (92, 93) and the expression of *TEP1* (44),
433 which positively regulates periostial hemocyte aggregation (14). Beyond immune
434 pathways, periostial hemocyte aggregation may also be under the influence of neuronal
435 and hormonal control. For example, injecting mosquitoes with the neuropeptide,
436 allatotropin, increases the number of periostial and non-periostial sessile hemocytes
437 (94). Therefore, the regulation of periostial hemocyte aggregation is not expected to be
438 limited to the IMD and JNK pathways.

439 To date, we have tested the involvement of several hemocyte-produced factors
440 on periostial hemocyte aggregation. However, the heart itself may produce
441 complementary factors that drive this immune response. For example, a fibroblast

442 growth factor is highly regulated in the heart and periostial hemocytes. Its ortholog in
443 *Drosophila*, called *Branchless*, is expressed in the heart and pericardial cells, and
444 regulates hemocyte differentiation in the lymph glands of the larval heart (95, 96).
445 Moreover, reducing the expression of the *Drosophila* cardiac extracellular matrix (ECM)
446 proteins, *Pericardin* and *Laminin A*, disrupts the formation of the cardiac ECM and
447 lowers the number of hemocytes on the heart (12, 97). These data suggest that the
448 heart and its associated structures facilitate the binding of circulating hemocytes to the
449 periostial regions.

450 The mosquito genome encodes three transglutaminase genes, and our RNAseq
451 experiment revealed that two of them are upregulated in the heart and periostial
452 hemocytes following infection. In *Drosophila*, transglutaminase negatively regulates the
453 IMD pathway by (i) crosslinking the transcription factor, Relish, into a polymer and (ii)
454 incorporating natural primary amines into the DNA binding site of Relish (38, 39). We
455 recently tested whether transglutaminases are involved in periostial responses in *A.*
456 *gambiae*, and found that *TGase3* – but not *TGase1* or *TGase2* – negatively regulates
457 periostial hemocyte aggregation during the early stages of infection and the
458 sequestration of melanin by periostial hemocytes during the later stages of infection
459 (40). Moreover, disrupting *TGase2* and *TGase3* has infection-dependent effects on the
460 heart rate (41). Combined, these data further support our conclusion that the IMD
461 pathway is a positive driver of heart-associated immune responses (Figure 6).

462 Heart-associated immune responses occur in insects from at least 16 different
463 taxonomic orders, including insects that are of agricultural, urban, and medical
464 importance (13). Understanding the genetic factors that drive periostial hemocyte

465 aggregation in *A. gambiae* sheds light on how this medically important insect and other
466 insects of societal importance fight the pathogens that invade them. Indeed, the TEP
467 gene family, the Nimrod gene family (Eater, Nimrod and Draper) and the JNK pathway
468 are conserved amongst insects (50, 98-100), and although some insects in the order
469 Hemiptera lack components of the IMD pathway, all insects queried to date still have a
470 functional IMD-based immune response (101-104). Therefore, we conclude that the
471 IMD and JNK pathways, together with TEP and Nimrod proteins, are primary regulators
472 of the heart-associated immune responses in insects.
473

474 **4. Materials and Methods**

475 *4.1. Mosquitoes, bacteria, infection, and replication*

476 *Anopheles gambiae,* Giles sensu stricto (G3; Diptera: Culicidae), were
477 maintained at 27 °C, 75% relative humidity, and a 12 hr:12 hr light:dark photoperiod
478 (105). Experiments were done using female adults fed 10% sucrose. After any
479 treatment, mosquitoes of a given treatment were housed together, returned to the
480 environmental chamber, and given access to 10% sucrose. Tetracycline resistant, GFP-
481 expressing *E. coli* (modified DH5α; GFP-*E. coli*) and *S. aureus* (RN6390) were grown in
482 Luria-Bertani (LB) and tryptic soy broth, respectively, at 37 °C in a shaking incubator.
483 Dilutions of the bacterial cultures were injected at the thoracic anepisternal cleft using a
484 Nanoject III (Drummond Scientific Company, Broomall, PA). The infection dose was
485 determined by plating the cultures and counting the colony forming units (CFUs).
486 In this study, a biological replicate is an independent experiment that utilizes
487 mosquitoes from an independent egg batch. A technical replicate is an experimental

488 resampling of a biological replicate. All data collected were included in the analysis; no
489 data were excluded.
490
491 *4.2. RNAseq: treatment, tissue collection, RNA isolation and library preparation*
492 Six-day-old mosquitoes were randomly divided into four groups: (i) naïve
493 (unmanipulated), (ii) injured by injecting 69 nL of sterile LB, (iii) infected by injecting 69
494 nL of GFP-*E. coli* (~75,779 CFUs), and (iv) infected by injecting 69 nL of *S. aureus*
495 (~39,451 CFUs). At 4 hr after treatment, three tissues were isolated: (i) the heart with
496 periostial hemocytes, (ii) hemolymph with circulating hemocytes, and (iii) the entire
497 abdomen. To isolate the heart, mosquitoes were bisected along the coronal plane in
498 RNase-free PBS, and the heart with the periostial hemocytes was resected by severing
499 the alary muscles and detaching it from the cuticle (7). To isolate circulating hemocytes,
500 hemolymph was perfused by making an incision in the last abdominal segment,
501 injecting RNase-free PBS into the hemocoel through the cervical membrane, and
502 collecting the first 2 drops that exited the abdomen (106). The abdomens were isolated
503 by bisecting mosquitoes on the transverse plane along the thoraco-abdominal junction.
504 To isolate RNA from hearts or abdomens, samples were homogenized in TRIzol
505 Reagent (Invitrogen, Carlsbad, CA), extracted following the TRIzol protocol, and
506 resuspended in Buffer RLT (Qiagen, Hilden, Germany) with 2% 2-mercaptoethanol. The
507 RNA was further purified using the RNeasy Micro Kit (Qiagen), DNase treated, and
508 eluted in RNase-free water. To isolate RNA from circulating hemocytes, perfused
509 hemolymph was collected in Buffer RLT and 2% 2-mercaptoethanol, and RNA was
510 isolated using the RNeasy Micro Kit as above.

511 No a priori statistical method was used to pre-determine sample sizes. The
512 number of RNAseq samples and biological replicates was determined prior to the
513 initiation of the study, and was based on our determination that three biological
514 replicates is a conservative approach to detect statistical differences (if any) in gene
515 expression. Three biological replicates were conducted; each heart sample contained
516 72 hearts, each hemolymph sample contained perfusate from 108 mosquitoes, and
517 each abdomen sample contained 36 abdomens.
518 The integrity and quantity of RNA was assessed on a 2100 Bioanalyzer (Agilent
519 Technologies, Santa Clara, CA) using an RNA 6000 Series II Nano kit for abdomen
520 samples and a Pico kit for the heart and hemolymph samples. The library for
521 sequencing was prepared using 1 µg of RNA and the NEBNext Ultra kit (New England
522 BioLabs, Ipswich, MA), according to the protocol for low-input samples. Library quality
523 and concentration were assessed using a DNA 1000 Series II kit on the 2100
524 Bioanalyzer.
525
526 *4.3. RNAseq: Illumina sequencing and differential gene expression analysis*
527 All 36 samples – 4 treatments, 3 tissue types and 3 biological replicates – were
528 sequenced across 3 lanes on an Illumina HiSeq 3000 (paired-end, 75 base pair read) at
529 Vanderbilt University's Vantage facility. Reads were mapped to the *A. gambiae* genome
530 (AgamP4.7) by STAR (107, 108). The number of uniquely mapped reads per sample
531 averaged 23,698,077 (range: 18,487,153 – 31,487,002), which represented 94.03% of
532 the total reads in a sample. Differential expression was calculated based on reads per
533 kilobase per million by DESeq2 (109). Genes were considered significantly regulated at

534 $\log_2$ fold change ⩾ 2 or $\log_2$ fold change ⩽ -2 and the Benjamini–Hochberg adjusted P
535 < 0.05. RNAseq results are presented in Dataset S1, which includes read counts and
536 log2 fold changes. Using four-fold expression difference as the criterion, together with
537 experimental replication and statistical validation, is a conservative approach that is
538 proven to yield accurate and reliable results (110). RNAseq data were deposited into
539 NCBI (https://www.ncbi.nlm.nih.gov) as SRA data PRJNA730047.
540

541 *4.4. Double-stranded RNA (dsRNA) synthesis and RNA interference (RNAi)*

542 Double-stranded RNA was synthesized for *rel2*, *caspar*, *PGRP-LA*, *JNK1* and
543 *JNK3*, and *puc*. *A. gambiae* cDNA was amplified by PCR using gene-specific primers
544 with T7 promoter tags (Table S6). dsRNA was synthesis using the MEGAscript T7 Kit
545 (Applied Biosystems) as described (14, 15). As a negative control, dsRNA was
546 synthesized for the non-mosquito gene, *bla(Ap^R)*, using DNA from *E. coli* BL21(DE3)
547 containing the pET-46 plasmid as template (EMD Chemicals, Gibbstown, NJ) (14, 15).
548 Two- or three-day-old mosquitoes were intrathoracically injected 300 ng of
549 dsRNA to initiate systemic gene silencing. Four days later, mosquitoes were divided into
550 two groups for phenotypic analyses: (i) uninfected and (ii) infected with GFP-*E. coli*
551 (~16,528 CFUs). Injured mosquitoes were not included in the experiments because
552 injury does not induce periostial hemocyte aggregation (4-6). RNAi efficiency of the
553 targeted genes and mRNA abundance of the downstream effector genes *TEP1*, *cec3*
554 and *def1* was determined by qPCR (14). Briefly, RNA was isolated using TRIzol from 10
555 whole bodies for each time and treatment, purified, and used for cDNA synthesis using
556 the SuperScript III First-Strand Synthesis System for RT-PCR (Invitrogen) as described

557 (14, 15). qPCR was conducted using gene-specific primers (Table S6) and Power
558 SYBR Green PCR Master Mix (Applied Biosystems, Foster City, CA) on a Bio Rad CFX
559 Connect Real-Time Detection System (Hercules, CA). Relative quantification was
560 conducted using the $2^{-\Delta\Delta C_T}$ method, with *RpS7* as the reference and *RpS17* as a control
561 (111). Two to three biological replicates were conducted per gene, and the value for
562 each biological replicate is the average of two or three technical replicates.
563

564 *4.5. Fluorescence labeling and mosquito dissection*

565 Hemocytes were labeled with the Vybrant CM-DiI Cell-Labeling Solution
566 (Invitrogen) as we described (5). Briefly, live mosquitoes were injected ~0.4 µL of 67 µM
567 CM-DiI and 1.08 mM Hoechst 33342 (nuclear stain; Invitrogen) in PBS, incubated at
568 27 °C for 20 min, and injected 16% paraformaldehyde. Ten min later, abdomens were
569 bisected along a coronal plane, and the dorsal portions containing the heart and
570 periostial hemocytes were mounted on glass slides using Aqua-Poly/Mount
571 (Polysciences; Warrington, PA). CM-DiI stains live hemocytes, and we have used this
572 technique to monitor hemocyte location, number and migration, as well as hemocyte-
573 mediated phagocytosis and melanization (4-9, 13-15, 40).
574

575 *4.6. Microscopy and image acquisition*

576 Specimens were imaged on a Nikon Eclipse Ni-E compound microscope
577 connected to a Nikon Digital Sight DS-Qi1 camera and Advanced Research NIS
578 Elements software (Nikon, Tokyo, Japan). Z-stacks for bright field, red fluorescence
579 (hemocytes), green fluorescence (GFP-*E. coli*) and blue fluorescence (nuclei) were

580 acquired using a linear encoded Z-motor. Specific channels were selected and all
581 images within a stack were combined into a two-dimensional image using the Extended
582 Depth of Focus (EDF) function.
583
584 *4.7. Quantification of hemocytes*
585 Hemocytes, labeled with both CM-DiI and Hoechst 33342, were counted
586 manually by examining all images within a Z-stack (14). A cell was a periostial
587 hemocyte if adjacent to an ostium, and a non-periostial sessile hemocyte if attached to
588 the abdominal wall outside of a periostial region (4, 5). Periostial hemocytes were
589 counted within abdominal segments 2-7 (all abdominal periostial regions) whereas non-
590 periostial sessile hemocytes were only counted on the tergum of segments 4 and 5.
591 Hemocytes were not counted on the aorta, the thoraco-abdominal ostia or the excurrent
592 openings because few hemocytes are there, and infection does not induce aggregation
593 at those locations (7, 8). Data were analyzed by two-way ANOVA, followed by Dunnett's
594 multiple comparison test, with ds*bla(Ap^R)* mosquitoes as the reference (Prism 9,
595 GraphPad Software, San Diego, CA). Data for RNAi phenotypic experiments are from
596 individual mosquitoes, which were sampled across three to four biological trials. The
597 exception is experiments for PGRP-LA, where mosquitoes were sampled across two
598 biological trials.
599
600 *4.8. Quantification of GFP-E. coli and melanin at the periostial regions*
601 In NIS-Elements, each periostial region in an EDF image was delineated using
602 the ROI tool. GFP-*E. coli* at the periostial regions was calculated by measuring the area

603 of pixels with intensities above a threshold that distinguished GFP-*E. coli* from
604 background fluorescence (14). Melanin was quantified by measuring the area of pixels
605 with intensities below a threshold that distinguished dark melanized areas from non-
606 melanized areas (14). For each mosquito, measurements from all ROIs were added.
607 Data were analyzed by two-way ANOVA, followed by Dunnett's multiple comparison
608 test, with ds*bla(Ap^R)* mosquitoes as the reference.
609
610 *4.9. Quantification of bacterial infection intensity*
611 Mosquitoes that were infected with tetracycline resistant GFP-*E. coli* for 4 or 24
612 hr were homogenized individually in PBS. A dilution of the homogenate was spread on
613 LB agar containing tetracycline, and plates were incubated overnight at 37 °C. The
614 CFUs were counted and used to calculate infection intensity. Data were analyzed by
615 two-way ANOVA, followed by Dunnett's multiple comparison test, with ds*bla(Ap^R)*
616 mosquitoes as the reference. For *rel2* and *caspar* RNAi mosquitoes, data were first $\log_2$
617 transformed to achieve normality, and then analyzed by two-way ANOVA.
618
619 **Data accessibility**
620 The datasets generated and analyzed during the current study are available in an
621 accompanying supplementary dataset file.
622
623 **Author's contributions**
624 Conceptualized and designed the research: YY, LTS, JFH; Performed the research: YY,
625 LTS, TYE; Contributed resources: JAC, JFH; Analyzed data: YY, LTS, DCR, JFH;

Wrote the original draft of the paper: YY, JFH; Administered the project and acquired funding: JFH.

Competing interests

The authors declare that there are no conflicts or competing interests.

Funding

This work was supported by U.S. National Science Foundation grants IOS-1456844 and IOS-1949145 to J.F.H.

Acknowledgments

We thank S. Williams, J. Sanner, C. Meier, L. Martin and L. Jabbur for useful discussions and commenting on this manuscript.

640 **References**
641

642 1. Hillyer JF. Insect immunology and hematopoiesis. Dev Comp Immunol.
643 2016;58:102-18.
644 2. Strand M. The insect cellular immune response. Insect Sci. 2008;15(1):1-14.
645 3. Hillyer JF, Strand MR. Mosquito hemocyte-mediated immune responses. Curr
646 Opin Insect Sci. 2014;3:14-21.
647 4. King JG, Hillyer JF. Spatial and temporal in vivo analysis of circulating and sessile
648 immune cells in mosquitoes: hemocyte mitosis following infection. BMC Biol.
649 2013;11:55.
650 5. King JG, Hillyer JF. Infection-induced interaction between the mosquito circulatory
651 and immune systems. PLoS Pathog. 2012;8(11):e1003058.
652 6. Sigle LT, Hillyer JF. Mosquito hemocytes preferentially aggregate and
653 phagocytose pathogens in the periostial regions of the heart that experience the
654 most hemolymph flow. Dev Comp Immunol. 2016;55:90-101.
655 7. Sigle LT, Hillyer JF. Mosquito hemocytes associate with circulatory structures that
656 support intracardiac retrograde hemolymph flow. Front Physiol. 2018;9:1187.
657 8. Sigle LT, Hillyer JF. Structural and functional characterization of the contractile
658 aorta and associated hemocytes of the mosquito *Anopheles gambiae*. J Exp Biol.
659 2018;221(Pt 12):jeb181107.
660 9. League GP, Hillyer JF. Functional integration of the circulatory, immune, and
661 respiratory systems in mosquito larvae: pathogen killing in the hemocyte-rich
662 tracheal tufts. BMC Biol. 2016;14:78.
663 10. Hernández-Martínez S, Lanz-Mendoza H, Martínez-Barnetche J, Rodríguez MH.
664 Antimicrobial properties of *Anopheles albimanus* pericardial cells. Cell Tissue Res.
665 2013;351(1):127-37.
666 11. da Silva R, da Silva SR, Lange AB. The regulation of cardiac activity by nitric oxide
667 (NO) in the Vietnamese stick insect, *Baculum extradentatum*. Cell Signal.
668 2012;24(6):1344-50.
669 12. Ghosh S, Singh A, Mandal S, Mandal L. Active hematopoietic hubs in *Drosophila*
670 adults generate hemocytes and contribute to immune response. Dev Cell.
671 2015;33(4):478-88.
672 13. Yan Y, Hillyer JF. The immune and circulatory systems are functionally integrated
673 across insect evolution. Sci Adv. 2020;6(48):eabb3164.
674 14. Yan Y, Hillyer JF. Complement-like proteins TEP1, TEP3 and TEP4 are positive
675 regulators of periostial hemocyte aggregation in the mosquito *Anopheles gambiae*.
676 Insect Biochem Mol Biol. 2019;107:1-9.
677 15. Sigle LT, Hillyer JF. *Eater* and *draper* are involved in the periostial haemocyte
678 immune response in the mosquito *Anopheles gambiae*. Insect Mol Biol.
679 2018;27(4):429-38.
680 16. Zhang W, Tettamanti G, Bassal T, Heryanto C, Eleftherianos I, Mohamed A.
681 Regulators and signalling in insect antimicrobial innate immunity: Functional
682 molecules and cellular pathways. Cell Signal. 2021;83:110003.
683 17. Shaw WR, Catteruccia F. Vector biology meets disease control: using basic
684 research to fight vector-borne diseases. Nat Microbiol. 2019;4(1):20-34.

685 18. King JG. Developmental and comparative perspectives on mosquito immunity. Dev
686 Comp Immunol. 2020;103:103458.
687 19. Banerjee U, Girard JR, Goins LM, Spratford CM. *Drosophila* as a genetic model for
688 hematopoiesis. Genetics. 2019;211(2):367-417.
689 20. Schmid MR, Anderl I, Vo HT, Valanne S, Yang H, Kronhamn J, et al. Genetic
690 screen in *Drosophila* larvae links *ird1* function to Toll signaling in the fat body and
691 hemocyte motility. PLoS One. 2016;11(7):e0159473.
692 21. Rämet M, Manfruelli P, Pearson A, Mathey-Prevot B, Ezekowitz RA. Functional
693 genomic analysis of phagocytosis and identification of a *Drosophila* receptor for *E.*
694 *coli*. Nature. 2002;416(6881):644-8.
695 22. Bahia AC, Kubota MS, Tempone AJ, Araújo HR, Guedes BA, Orfanó AS, et al. The
696 JAK-STAT pathway controls *Plasmodium vivax* load in early stages of *Anopheles*
697 *aquasalis* infection. PLoS Negl Trop Dis. 2011;5(11):e1317.
698 23. Souza-Neto JA, Sim S, Dimopoulos G. An evolutionary conserved function of the
699 JAK-STAT pathway in anti-dengue defense. Proc Natl Acad Sci U S A.
700 2009;106(42):17841-6.
701 24. Minakhina S, Tan W, Steward R. JAK/STAT and the GATA factor Pannier control
702 hemocyte maturation and differentiation in *Drosophila*. Dev Biol. 2011;352(2):308-
703 16.
704 25. Krzemień J, Dubois L, Makki R, Meister M, Vincent A, Crozatier M. Control of
705 blood cell homeostasis in *Drosophila* larvae by the posterior signalling centre.
706 Nature. 2007;446(7133):325-8.
707 26. Gendrin M, Turlure F, Rodgers FH, Cohuet A, Morlais I, Christophides GK. The
708 peptidoglycan recognition proteins PGRPLA and PGRPLB regulate
709 *Anopheles* immunity to bacteria and affect infection by *Plasmodium*. J Innate
710 Immun. 2017;9(4):333-42.
711 27. Myllymäki H, Valanne S, Rämet M. The *Drosophila* imd signaling pathway. J
712 Immunol. 2014;192(8):3455-62.
713 28. Garver LS, Bahia AC, Das S, Souza-Neto JA, Shiao J, Dong Y, et al. *Anopheles*
714 Imd pathway factors and effectors in infection intensity-dependent anti-
715 *Plasmodium* action. PLoS Pathog. 2012;8(6):e1002737.
716 29. Meister S, Kanzok SM, Zheng XL, Luna C, Li TR, Hoa NT, et al. Immune signaling
717 pathways regulating bacterial and malaria parasite infection of the mosquito
718 *Anopheles gambiae*. Proc Natl Acad Sci U S A. 2005;102(32):11420-5.
719 30. Garver LS, Dong Y, Dimopoulos G. Caspar controls resistance to *Plasmodium*
720 *falciparum* in diverse anopheline species. PLoS Pathog. 2009;5(3):e1000335.
721 31. Luna C, Hoa NT, Lin H, Zhang L, Nguyen HL, Kanzok SM, et al. Expression of
722 immune responsive genes in cell lines from two different Anopheline species.
723 Insect Mol Biol. 2006;15(6):721-9.
724 32. Boutros M, Agaisse H, Perrimon N. Sequential activation of signaling pathways
725 during innate immune responses in *Drosophila*. Dev Cell. 2002;3(5):711-22.
726 33. Souvannaseng L, Hun LV, Baker H, Klyver JM, Wang B, Pakpour N, et al.
727 Inhibition of JNK signaling in the Asian malaria vector *Anopheles stephensi*
728 extends mosquito longevity and improves resistance to *Plasmodium falciparum*
729 infection. PLoS Pathog. 2018;14(11):e1007418.

730 34. Silverman N, Zhou R, Erlich RL, Hunter M, Bernstein E, Schneider D, et al.
731 Immune activation of NF-kappaB and JNK requires *Drosophila* TAK1. J Biol Chem.
732 2003;278(49):48928-34.
733 35. Zhuang ZH, Sun L, Kong L, Hu JH, Yu MC, Reinach P, et al. *Drosophila* TAB2 is
734 required for the immune activation of JNK and NF-kappaB. Cell Signal.
735 2006;18(7):964-70.
736 36. Wong CO, Gregory S, Hu H, Chao Y, Sepúlveda VE, He Y, et al. Lysosomal
737 degradation is required for sustained phagocytosis of bacteria by macrophages.
738 Cell Host Microbe. 2017;21(6):719-30.e6.
739 37. Bretscher A, Honti V, Binggeli O, Burri O, Poidevin M, Kurucz E, et al. The Nimrod
740 transmembrane receptor Eater is required for hemocyte attachment to the sessile
741 compartment in *Drosophila melanogaster*. Biol Open. 2015;4(3):355-63.
742 38. Shibata T, Sekihara S, Fujikawa T, Miyaji R, Maki K, Ishihara T, et al.
743 Transglutaminase-catalyzed protein-protein cross-linking suppresses the activity of
744 the NF-κB-like transcription factor relish. Sci Signal. 2013;6(285):ra61.
745 39. Maki K, Shibata T, Kawabata S. Transglutaminase-catalyzed incorporation of
746 polyamines masks the DNA-binding region of the transcription factor Relish. J Biol
747 Chem. 2017;292(15):6369-80.
748 40. Yan Y, Ramakrishnan A, Estévez-Lao TY, Hillyer JF. Transglutaminase 3
749 negatively regulates immune responses on the heart of the mosquito, *Anopheles*
750 *gambiae*. Sci Rep. 2022;12(1):6715.
751 41. Ramakrishnan A, Hillyer JF. Silencing transglutaminase genes *TGase2* and
752 *TGase3* has infection-dependent effects on the heart rate of the mosquito
753 *Anopheles gambiae*. Insects. 2022;13(7):582.
754 42. Etchegaray JI, Timmons AK, Klein AP, Pritchett TL, Welch E, Meehan TL, et al.
755 Draper acts through the JNK pathway to control synchronous engulfment of dying
756 germline cells by follicular epithelial cells. Development. 2012;139(21):4029-39.
757 43. Weavers H, Evans IR, Martin P, Wood W. Corpse engulfment generates a
758 molecular memory that primes the macrophage inflammatory response. Cell.
759 2016;165(7):1658-71.
760 44. Frolet C, Thoma M, Blandin S, Hoffmann J, Levashina E. Boosting NF-kappa B-
761 dependent basal immunity of *Anopheles gambiae* aborts development of
762 *Plasmodium berghei*. Immunity. 2006;25(4):677-85.
763 45. Feng Y, Chen L, Gao L, Dong L, Wen H, Song X, et al. Rapamycin inhibits
764 pathogen transmission in mosquitoes by promoting immune activation. PLoS
765 Pathog. 2021;17(2):e1009353.
766 46. Huang CY, Chou SY, Bartholomay LC, Christensen BM, Chen CC. The use of
767 gene silencing to study the role of dopa decarboxylase in mosquito melanization
768 reactions. Insect Mol Biol. 2005;14(3):237-44.
769 47. Paskewitz SM, Andreev O. Silencing the genes for dopa decarboxylase or
770 dopachrome conversion enzyme reduces melanization of foreign targets in
771 *Anopheles gambiae*. Comp Biochem Physiol B Biochem Mol Biol.
772 2008;150(4):403-8.
773 48. Gendrin M, Zaidman-Rémy A, Broderick NA, Paredes J, Poidevin M, Roussel A, et
774 al. Functional analysis of PGRP-LA in *Drosophila* immunity. PLoS One.
775 2013;8(7):e69742.

776 49. Werner T, Liu G, Kang D, Ekengren S, Steiner H, Hultmark D. A family of
777 peptidoglycan recognition proteins in the fruit fly *Drosophila melanogaster*. Proc
778 Natl Acad Sci U S A. 2000;97(25):13772-7.
779 50. Horton AA, Wang B, Camp L, Price MS, Arshi A, Nagy M, et al. The mitogen-
780 activated protein kinome from *Anopheles gambiae*: identification, phylogeny and
781 functional characterization of the ERK, JNK and p38 MAP kinases. BMC
782 Genomics. 2011;12:574.
783 51. Garver LS, de Almeida Oliveira G, Barillas-Mury C. The JNK pathway is a key
784 mediator of *Anopheles gambiae* antiplasmodial immunity. PLoS Pathog.
785 2013;9(9):e1003622.
786 52. Kwon H, Smith R. Chemical depletion of phagocytic immune cells in *Anopheles*
787 *gambiae* reveals dual roles of mosquito hemocytes in anti-*Plasmodium* immunity.
788 Proc Natl Acad Sci U S A. 2019;116(28):14119-28.
789 53. Pinto SB, Lombardo F, Koutsos AC, Waterhouse RM, McKay K, An C, et al.
790 Discovery of *Plasmodium* modulators by genome-wide analysis of circulating
791 hemocytes in *Anopheles gambiae*. Proc Natl Acad Sci U S A. 2009;106(50):21270-
792 5.
793 54. Baton LA, Robertson A, Warr E, Strand MR, Dimopoulos G. Genome-wide
794 transcriptomic profiling of *Anopheles gambiae* hemocytes reveals pathogen-
795 specific signatures upon bacterial challenge and *Plasmodium berghei* infection.
796 BMC Genomics. 2009;10:257.
797 55. Thomas T, De TD, Sharma P, Lata S, Saraswat P, Pandey KC, et al.
798 Hemocytome: deep sequencing analysis of mosquito blood cells in Indian malarial
799 vector *Anopheles stephensi*. Gene. 2016;585(2):177-90.
800 56. Bartholomay LC, Cho WL, Rocheleau TA, Boyle JP, Beck ET, Fuchs JF, et al.
801 Description of the transcriptomes of immune response-activated hemocytes from
802 the mosquito vectors *Aedes aegypti* and *Armigeres subalbatus*. Infect Immun.
803 2004;72(7):4114-26.
804 57. Choi YJ, Fuchs JF, Mayhew GF, Yu HE, Christensen BM. Tissue-enriched
805 expression profiles in *Aedes aegypti* identify hemocyte-specific transcriptome
806 responses to infection. Insect Biochem Mol Biol. 2012;42(10):729-38.
807 58. Rani J, Chauhan C, Das De T, Kumari S, Sharma P, Tevatiya S, et al. Hemocyte
808 RNA-Seq analysis of Indian malarial vectors *Anopheles stephensi* and *Anopheles*
809 *culicifacies*: From similarities to differences. Gene. 2021;798:145810.
810 59. Severo M, Landry J, Lindquist R, Goosmann C, Brinkmann V, Collier P, et al.
811 Unbiased classification of mosquito blood cells by single-cell genomics and high-
812 content imaging. Proc Natl Acad Sci U S A. 2018;115(32):E7568-E77.
813 60. Raddi G, Barletta ABF, Efremova M, Ramirez JL, Cantera R, Teichmann SA, et al.
814 Mosquito cellular immunity at single-cell resolution. Science.
815 2020;369(6507):1128-32.
816 61. Kwon H, Mohammed M, Franzén O, Ankarklev J, Smith RC. Single-cell analysis of
817 mosquito hemocytes identifies signatures of immune cell subtypes and cell
818 differentiation. Elife. 2021;10:e66192.
819 62. Márkus R, Laurinyecz B, Kurucz E, Honti V, Bajusz I, Sipos B, et al. Sessile
820 hemocytes as a hematopoietic compartment in *Drosophila melanogaster*. Proc Natl
821 Acad Sci U S A. 2009;106(12):4805-9.

822 63. Leitão AB, Sucena É. *Drosophila* sessile hemocyte clusters are true hematopoietic
823 tissues that regulate larval blood cell differentiation. Elife. 2015;4:e06166.
824 64. Babcock DT, Brock AR, Fish GS, Wang Y, Perrin L, Krasnow MA, et al. Circulating
825 blood cells function as a surveillance system for damaged tissue in *Drosophila*
826 larvae. Proc Natl Acad Sci U S A. 2008;105(29):10017-22.
827 65. Horn L, Leips J, Starz-Gaiano M. Phagocytic ability declines with age in adult
828 *Drosophila* hemocytes. Aging Cell. 2014;13(4):719-28.
829 66. Kocks C, Cho J, Nehme N, Ulvila J, Pearson A, Meister M, et al. Eater, a
830 transmembrane protein mediating phagocytosis of bacterial pathogens in
831 *Drosophila*. Cell. 2005;123(2):335-46.
832 67. Moita LF, Wang-Sattler R, Michel K, Zimmermann T, Blandin S, Levashina EA, et
833 al. In vivo identification of novel regulators and conserved pathways of
834 phagocytosis in *A. gambiae*. Immunity. 2005;23(1):65-73.
835 68. Dong Y, Das S, Cirimotich C, Souza-Neto JA, McLean KJ, Dimopoulos G.
836 Engineered *Anopheles* immunity to *Plasmodium* infection. PLoS Pathog.
837 2011;7(12):e1002458.
838 69. Mantuano E, Jo M, Gonias SL, Campana WM. Low density lipoprotein receptor-
839 related protein (LRP1) regulates Rac1 and RhoA reciprocally to control Schwann
840 cell adhesion and migration. J Biol Chem. 2010;285(19):14259-66.
841 70. Moita LF, Vriend G, Mahairaki V, Louis C, Kafatos FC. Integrins of *Anopheles*
842 *gambiae* and a putative role of a new beta integrin, BINT2, in phagocytosis of *E.*
843 *coli*. Insect Biochem Mol Biol. 2006;36(4):282-90.
844 71. Rabiej VK, Pflanzner T, Wagner T, Goetze K, Storck SE, Eble JA, et al. Low
845 density lipoprotein receptor-related protein 1 mediated endocytosis of β1-integrin
846 influences cell adhesion and cell migration. Exp Cell Res. 2016;340(1):102-15.
847 72. Mitri C, Jacques JC, Thiery I, Riehle MM, Xu J, Bischoff E, et al. Fine pathogen
848 discrimination within the APL1 gene family protects *Anopheles gambiae* against
849 human and rodent malaria species. PLoS Pathog. 2009;5(9):e1000576.
850 73. Dong Y, Simões ML, Dimopoulos G. Versatile transgenic multistage effector-gene
851 combinations for *Plasmodium falciparum* suppression in *Anopheles*. Sci Adv.
852 2020;6(20):eaay5898.
853 74. Meister S, Agianian B, Turlure F, Relógio A, Morlais I, Kafatos FC, et al. *Anopheles*
854 *gambiae* PGRPLC-mediated defense against bacteria modulates infections with
855 malaria parasites. PLoS Pathog. 2009;5(8):e1000542.
856 75. Khan MB, Liew JW, Leong CS, Lau YL. Role of NF-kβ factor Rel2 during
857 *Plasmodium falciparum* and bacterial infection in *Anopheles dirus*. Parasit Vectors.
858 2016;9(1):525.
859 76. Dekmak AS, Yang X, Zu Dohna H, Buchon N, Osta MA. The route of infection
860 influences the contribution of key immunity genes to antibacterial defense in
861 *Anopheles gambiae*. J Innate Immun. 2021;13(2):107-26.
862 77. Kambris Z, Blagborough AM, Pinto SB, Blagrove MS, Godfray HC, Sinden RE, et
863 al. *Wolbachia* stimulates immune gene expression and inhibits *plasmodium*
864 development in *Anopheles gambiae*. PLoS Pathog. 2010;6(10):e1001143.
865 78. Schnitger AK, Kafatos FC, Osta MA. The melanization reaction is not required for
866 survival of *Anopheles gambiae* mosquitoes after bacterial infections. J Biol Chem.
867 2007;282(30):21884-8.

868 79. Ramphul U, Garver L, Molina-Cruz A, Canepa G, Barillas-Mury C. *Plasmodium*
869 *falciparum* evades mosquito immunity by disrupting JNK-mediated apoptosis of
870 invaded midgut cells. Proc Natl Acad Sci U S A. 2015;112(5):1273-80.
871 80. Peirce MJ, Mitchell SN, Kakani EG, Scarpelli P, South A, Shaw WR, et al. JNK
872 signaling regulates oviposition in the malaria vector *Anopheles gambiae*. Sci Rep.
873 2020;10(1):14344.
874 81. Nsango S, Pompon J, Xie T, Rademacher A, Fraiture M, Thoma M, et al. AP-
875 1/Fos-TGase2 axis mediates wounding-induced *Plasmodium falciparum* killing in
876 *Anopheles gambiae*. J Biol Chem. 2013;288(22):16145-54.
877 82. Chowdhury A, Modahl C, Tan S, Xiang B, Misse D, Vial T, et al. JNK pathway
878 restricts DENV2, ZIKV and CHIKV infection by activating complement and
879 apoptosis in mosquito salivary glands. Plos Pathogens. 2020;16(8):e1008754.
880 83. Williams MJ, Wiklund ML, Wikman S, Hultmark D. Rac1 signalling in the
881 *Drosophila* larval cellular immune response. J Cell Sci. 2006;119(Pt 10):2015-24.
882 84. Zettervall CJ, Anderl I, Williams MJ, Palmer R, Kurucz E, Ando I, et al. A directed
883 screen for genes involved in *Drosophila* blood cell activation. Proc Natl Acad Sci U
884 S A. 2004;101(39):14192-7.
885 85. Ma L, Liu L, Zhao Y, Yang L, Chen C, Li Z, et al. JNK pathway plays a key role in
886 the immune system of the pea aphid and is regulated by microRNA-184. PLoS
887 Pathog. 2020;16(6):e1008627.
888 86. Macdonald JM, Doherty J, Hackett R, Freeman MR. The c-Jun kinase signaling
889 cascade promotes glial engulfment activity through activation of draper and
890 phagocytic function. Cell Death Differ. 2013;20(9):1140-8.
891 87. Manaka J, Kuraishi T, Shiratsuchi A, Nakai Y, Higashida H, Henson P, et al.
892 Draper-mediated and phosphatidylserine-independent phagocytosis of apoptotic
893 cells by *Drosophila* hemocytes/macrophages. J Biol Chem. 2004;279(46):48466-
894 76.
895 88. Evans IR, Rodrigues FS, Armitage EL, Wood W. Draper/CED-1 mediates an
896 ancient damage response to control inflammatory blood cell migration in vivo. Curr
897 Biol. 2015;25(12):1606-12.
898 89. Levashina EA, Moita LF, Blandin S, Vriend G, Lagueux M, Kafatos FC. Conserved
899 role of a complement-like protein in phagocytosis revealed by dsRNA knockout in
900 cultured cells of the mosquito, *Anopheles gambiae*. Cell. 2001;104(5):709-18.
901 90. Nagaosa K, Okada R, Nonaka S, Takeuchi K, Fujita Y, Miyasaka T, et al. Integrin
902 βv-mediated phagocytosis of apoptotic cells in *Drosophila* embryos. J Biol Chem.
903 2011;286(29):25770-7.
904 91. Chakrabarti S, Dudzic JP, Li X, Collas EJ, Boquete JP, Lemaitre B. Remote control
905 of intestinal stem cell activity by haemocytes in *Drosophila*. PLoS Genet.
906 2016;12(5):e1006089.
907 92. Qiu P, Pan PC, Govind S. A role for the *Drosophila* Toll/Cactus pathway in larval
908 hematopoiesis. Development. 1998;125(10):1909-20.
909 93. Chiu H, Ring BC, Sorrentino RP, Kalamarz M, Garza D, Govind S. dUbc9
910 negatively regulates the Toll-NF-kappa B pathways in larval hematopoiesis and
911 drosomycin activation in *Drosophila*. Dev Biol. 2005;288(1):60-72.

912 94. Hernández-Martínez S, Sánchez-Zavaleta M, Brito K, Herrera-Ortiz A, Ons S,
913 Noriega FG. Allatotropin: A pleiotropic neuropeptide that elicits mosquito immune
914 responses. PLoS One. 2017;12(4):e0175759.
915 95. Destalminil-Letourneau M, Morin-Poulard I, Tian Y, Vanzo N, Crozatier M. The
916 vascular niche controls *Drosophila* hematopoiesis via fibroblast growth factor
917 signaling. Elife. 2021;10:e64672.
918 96. Dragojlovic-Munther M, Martinez-Agosto JA. Extracellular matrix-modulated
919 Heartless signaling in *Drosophila* blood progenitors regulates their differentiation
920 via a Ras/ETS/FOG pathway and target of rapamycin function. Dev Biol.
921 2013;384(2):313-30.
922 97. Cevik D, Acker M, Michalski C, Jacobs JR. Pericardin, a *Drosophila* collagen,
923 facilitates accumulation of hemocytes at the heart. Dev Biol. 2019;454(1):52-65.
924 98. Blandin S, Levashina EA. Thioester-containing proteins and insect immunity. Mol
925 Immunol. 2004;40(12):903-8.
926 99. Bou Aoun R, Hetru C, Troxler L, Doucet D, Ferrandon D, Matt N. Analysis of
927 thioester-containing proteins during the innate immune response of *Drosophila*
928 *melanogaster*. J Innate Immun. 2011;3(1):52-64.
929 100. Somogyi K, Sipos B, Pénzes Z, Kurucz E, Zsámboki J, Hultmark D, et al. Evolution
930 of genes and repeats in the Nimrod superfamily. Mol Biol Evol. 2008;25(11):2337-
931 47.
932 101. Nishide Y, Kageyama D, Yokoi K, Jouraku A, Tanaka H, Futahashi R, et al.
933 Functional crosstalk across IMD and Toll pathways: insight into the evolution of
934 incomplete immune cascades. Proc Biol Sci. 2019;286(1897):20182207.
935 102. Salcedo-Porras N, Guarneri A, Oliveira PL, Lowenberger C. *Rhodnius prolixus*:
936 Identification of missing components of the IMD immune signaling pathway and
937 functional characterization of its role in eliminating bacteria. PLoS One.
938 2019;14(4):e0214794.
939 103. Mesquita RD, Vionette-Amaral RJ, Lowenberger C, Rivera-Pomar R, Monteiro FA,
940 Minx P, et al. Genome of *Rhodnius prolixus*, an insect vector of Chagas disease,
941 reveals unique adaptations to hematophagy and parasite infection. Proc Natl Acad
942 Sci U S A. 2015;112(48):14936-41.
943 104. Gerardo NM, Altincicek B, Anselme C, Atamian H, Barribeau SM, de Vos M, et al.
944 Immunity and other defenses in pea aphids, *Acyrthosiphon pisum*. Genome Biol.
945 2010;11(2):R21.
946 105. Glenn JD, King JG, Hillyer JF. Structural mechanics of the mosquito heart and its
947 function in bidirectional hemolymph transport. J Exp Biol. 2010;213(4):541-50.
948 106. Hillyer JF, Christensen BM. Characterization of hemocytes from the yellow fever
949 mosquito, *Aedes aegypti*. Histochem Cell Biol. 2002;117(5):431-40.
950 107. Dobin A, Davis CA, Schlesinger F, Drenkow J, Zaleski C, Jha S, et al. STAR:
951 ultrafast universal RNA-seq aligner. Bioinformatics. 2013;29(1):15-21.
952 108. Giraldo-Calderón GI, Emrich SJ, MacCallum RM, Maslen G, Dialynas E, Topalis P,
953 et al. VectorBase: an updated bioinformatics resource for invertebrate vectors and
954 other organisms related with human diseases. Nucleic Acids Res.
955 2015;43(Database issue):D707-13.
956 109. Love MI, Huber W, Anders S. Moderated estimation of fold change and dispersion
957 for RNA-seq data with DESeq2. Genome Biol. 2014;15(12):550.

958 110. Everaert C, Luypaert M, Maag JLV, Cheng QX, Dinger ME, Hellemans J, et al.
959 Benchmarking of RNA-sequencing analysis workflows using whole-transcriptome
960 RT-qPCR expression data. Sci Rep. 2017;7(1):1559.
961 111. League GP, Estévez-Lao TY, Yan Y, Garcia-Lopez VA, Hillyer JF. *Anopheles*
962 *gambiae* larvae mount stronger immune responses against bacterial infection than
963 adults: evidence of adaptive decoupling in mosquitoes. Parasit Vectors.
964 2017;10(1):367.
965

966 **The IMD and JNK pathways drive the functional integration of the immune and**

967 **circulatory systems of mosquitoes**

968

969 Yan Yan [1], Leah T. Sigle [1], David C. Rinker [1], Tania Y. Estévez-Lao [1], John A. Capra [1,2]

970 and Julián F. Hillyer [1]*

971

972 [1] Department of Biological Sciences, Vanderbilt University, Nashville, TN, USA

973 [2] Bakar Computational Health Sciences Institute and Department of Epidemiology and

974 Biostatistics, University of California San Francisco. San Francisco, CA, USA

975 * julian.hillyer@vanderbilt.edu

976

977 **Supplementary tables and figures:**

978 • Tables S1-S6

979 • Figures S1-S8

980 **Table S1.** Upregulated genes in the heart with periostial hemocytes at 4 hr following

981 both GFP-*E. coli* and *S. aureus* infection.

			***E. coli* vs Injured**		***S. aureus* vs Injured**	
Gene ID	**Gene name**	**Gene description (if annotated)**	**Log2Foldchange**	**Adjusted P**	**Log2Foldchange**	**Adjusted P**
AGAP000694	*cec3*	cecropin anti-microbial peptide	2.72	8E-14	3.20	2E-19
AGAP000786			2.88	4E-06	3.12	2E-07
AGAP001160			3.03	3E-21	4.46	1E-47
AGAP001212	*PGRPLB*	peptidoglycan recognition protein (long)	3.10	2E-25	4.21	3E-47
AGAP001508			3.19	4E-07	5.03	2E-17
AGAP001563		glycerol kinase	2.58	7E-12	2.70	3E-13
AGAP001597			2.14	9E-04	2.14	6E-04
AGAP001610			4.07	2E-21	4.13	2E-22
AGAP001634			3.52	1E-14	2.48	1E-07
AGAP001648	*CLIPB17*	CLIP-domain serine protease	2.24	4E-10	3.01	3E-18
AGAP001828			2.13	2E-16	2.38	9E-21
AGAP002064			2.05	7E-18	2.29	1E-22
AGAP002065		alpha-tocopherol transfer protein	2.14	1E-13	2.64	3E-21
AGAP002291		ebony	2.81	1E-30	3.62	2E-51
AGAP002323			2.82	2E-11	3.31	4E-16
AGAP002331	*esp*	sodium-independent sulfate anion transporter	3.15	8E-20	2.94	1E-17
AGAP002359		carbonic anhydrase	2.62	2E-02	4.62	4E-06
AGAP002536			2.48	3E-13	2.75	1E-16
AGAP002883			2.28	3E-24	2.69	5E-34
AGAP003488		nucleotide exchange factor SIL1	2.02	2E-06	2.49	1E-09
AGAP004170			2.18	4E-21	2.73	8E-34
AGAP004181		Fibroblast growth factor	2.53	1E-06	2.40	4E-06
AGAP004826			3.04	4E-09	4.30	2E-18
AGAP005205	*PGRPLA*	peptidoglycan recognition protein (long)	2.36	7E-47	2.66	1E-60
AGAP005610			2.44	1E-06	4.99	2E-27
AGAP005839		MFS transporter, FLVCR family	3.65	4E-41	3.97	3E-49
AGAP006426		cyanogenic beta-glucosidase	2.65	2E-03	5.58	2E-13
AGAP006670		gamma-glutamyl hydrolase	2.31	8E-24	2.90	4E-38
AGAP006671			3.18	6E-18	3.85	2E-27
AGAP006674		chymotrypsin-like protease (Precursor)	2.93	2E-02	7.46	1E-12
AGAP006745			2.35	4E-29	2.78	3E-41
AGAP006747	*rel2*	NF-kappaB Relish-like transcription factor	2.00	2E-33	2.21	3E-41
AGAP007659			2.61	4E-15	3.57	1E-28
AGAP008279	*d7l2*	D7 long form salivary protein	16.43	2E-05	13.73	3E-04
AGAP008851		E3 ubiquitin-protein ligase mind-bomb	2.66	2E-26	2.95	8E-33
AGAP009091	*ddc*	dopa decarboxylase	3.96	2E-50	4.81	3E-75
AGAP009099	*TGase3*	Transglutaminase	3.98	2E-17	4.05	1E-18
AGAP009100	*TGase1*	Transglutaminase	3.20	3E-37	3.76	1E-51
AGAP009145			2.12	1E-13	3.03	4E-28
AGAP009213	*SRPN16*	serine protease inhibitor (serpin) 16	2.61	8E-13	3.75	1E-26
AGAP009214	*CLIPB11*	CLIP-domain serine protease	2.13	1E-06	3.71	2E-19
AGAP009460	*JNK3*	c-Jun N-terminal kinase	2.22	1E-04	3.47	1E-10
AGAP009985		4-nitrophenylphosphatase	2.19	3E-08	3.16	4E-17
AGAP010197		SPRY domain-containing SOCS box protein 1	2.31	2E-20	2.85	2E-31
AGAP010398		Flavin-containing monooxygenase FMO GS-OX-like 1	2.78	8E-08	5.85	1E-33
AGAP010934			2.94	1E-30	3.17	3E-36
AGAP011294	*def1*	defensin anti-microbial peptide	2.13	2E-05	2.70	1E-08
AGAP011326	*IAP2*	inhibitor of apoptosis 2	3.21	2E-38	3.29	1E-40
AGAP011588			2.60	2E-29	3.33	4E-49
AGAP011654		membrane dipeptidase	2.13	5E-05	3.58	3E-13
AGAP011764			2.71	5E-63	2.87	4E-71
AGAP011992		lysosomal acid lipase	2.72	7E-05	3.01	4E-06
AGAP012166			3.70	2E-13	2.92	8E-09
AGAP013506	*upd3a*	JAK/STAT pathway cytokine unpaired 3 variant A	3.89	2E-12	4.05	8E-14
AGAP028615	*nat5*	nutrient amino acid transporter 5	2.54	4E-10	4.28	2E-28

982
983
984

985 **Table S2.** Upregulated genes in the circulating hemocytes at 4 hr following both GFP-*E.*

986 *coli* and *S. aureus* infection.

			***E. coli* vs Injured**		***S. aureus* vs Injured**	
Gene ID	**Gene name**	**Gene description (if annotated)**	**Log2Foldchange**	**Adjusted P**	**Log2Foldchange**	**Adjusted P**
AGAP000899			3.31	3E-07	4.74	8E-16
AGAP001212	*PGRPLB*	peptidoglycan recognition protein (long)	2.68	2E-18	4.39	4E-51
AGAP001430			2.27	2E-18	3.39	7E-43
AGAP001508			2.06	3E-03	3.26	1E-07
AGAP002291		ebony	2.46	3E-23	3.73	2E-55
AGAP004115		cystinosin	2.07	5E-03	5.38	5E-18
AGAP005610			2.45	8E-08	4.09	7E-23
AGAP005639	*abcb2*	ATP-binding cassette transporter (ABC transporter) family B member 2	2.23	1E-12	3.47	1E-31
AGAP007651		growth arrest and DNA-damage-inducible protein	2.19	8E-11	3.30	2E-25
AGAP009091	*ddc*	dopa decarboxylase	2.06	2E-13	2.93	3E-28
AGAP010349			2.28	3E-05	3.50	1E-12
AGAP010387		alanine-glyoxylate aminotransferase	2.29	3E-03	3.54	3E-07
AGAP010571			2.43	5E-06	3.25	3E-11
AGAP010855		solute carrier family 45, member 1/2/4	3.24	7E-06	5.23	7E-16
AGAP011326	*IAP2*	inhibitor of apoptosis 2	2.26	2E-18	2.58	4E-25
AGAP011391			2.07	7E-07	3.62	8E-22
AGAP011588			2.43	7E-25	3.18	8E-45
AGAP011589			2.95	2E-02	3.46	3E-03
AGAP012565			3.58	7E-02	3.78	5E-02
AGAP013285	*ir7u*	ionotropic receptor IR7u	2.36	3E-03	3.46	9E-07
AGAP028615	*nat5*	nutrient amino acid transporter 5	2.27	9E-08	4.06	2E-25

987
988
989
990 **Table S3.** Upregulated genes in the abdomen at 4 hr following both GFP-*E. coli* and *S.*

991 *aureus* infection.

			***E. coli* vs Injured**		***S. aureus* vs Injured**	
Gene ID	**Gene name**	**Gene description (if annotated)**	**Log2Foldchange**	**Adjusted P**	**Log2Foldchange**	**Adjusted P**
AGAP001212	*PGRPLB*	peptidoglycan recognition protein (long)	3.22	4E-26	3.97	8E-41
AGAP001508			2.54	3E-04	4.63	5E-14
AGAP001610			3.33	1E-13	2.75	1E-09
AGAP001648	*CLIPB17*	CLIP-domain serine protease	2.04	8E-08	3.27	1E-20
AGAP002291		ebony	2.52	3E-24	2.47	1E-23
AGAP006670		gamma-glutamyl hydrolase	2.08	1E-18	2.33	9E-24
AGAP006745			2.06	8E-21	2.39	2E-28
AGAP007651		growth arrest and DNA-damage-inducible protein	2.17	2E-10	2.16	1E-10
AGAP007659			2.13	2E-09	2.45	7E-13
AGAP009145			2.18	2E-13	3.51	2E-36
AGAP010398		Flavin-containing monooxygenase FMO GS-OX-like 1	2.62	2E-06	5.93	3E-33
AGAP010934			2.59	6E-23	2.25	1E-17
AGAP011294	*def1*	defensin anti-microbial peptide	2.04	2E-04	2.39	3E-06
AGAP011326	*IAP2*	inhibitor of apoptosis 2	2.16	2E-16	2.17	8E-17
AGAP013348			2.40	4E-22	3.34	2E-43

992
993
994

995 **Table S4.** Downregulated genes in the heart with periostial hemocytes at 4 hr following

996 both GFP-*E. coli* and *S. aureus* infection.

			E. coli vs injury		*S. aureus* vs injury	
Gene ID	**Gene name**	**Gene description (if annotated)**	**Log2Foldchange**	**Adjusted P**	**Log2Foldchange**	**Adjusted P**
AGAP000313		alanine-glyoxylate aminotransferase 2-like	-2.19	2E-12	-2.24	3E-13
AGAP001009			-2.28	2E-04	-3.11	1E-05
AGAP001098		DAMOX	-2.25	8E-03	-2.73	1E-03
AGAP002429	*CYP314A1*	cytochrome P450	-2.46	1E-03	-3.41	2E-06
AGAP003494		sugar transporter ERD6-like 7	-2.75	1E-08	-2.63	3E-08
AGAP004248	*GPXH3*	glutathione peroxidase 3	-2.32	9E-05	-2.43	3E-05
AGAP004954		rhythmically expressed gene 2 protein	-2.10	7E-12	-2.30	3E-14
AGAP005498		Phospholipid scramblase	-2.13	4E-05	-2.90	4E-09
AGAP005499		dehydrogenase/reductase SDR family member 11 precursor	-2.53	4E-04	-3.33	4E-06
AGAP005752		glucosyl/glucuronosyl transferases	-2.29	2E-06	-2.33	7E-07
AGAP005753		glucosyl/glucuronosyl transferases	-2.55	2E-10	-2.60	9E-11
AGAP006576		malate/L-lactate dehydrogenase	-2.17	1E-21	-2.72	1E-33
AGAP008207	*CYP6Y2*	cytochrome P450	-2.43	2E-33	-2.63	1E-38
AGAP008467		solute carrier family 6 (neurotransmitter transporter, amino acid) member 5/7/	-3.02	2E-17	-2.74	2E-15
AGAP008593			-2.47	3E-02	-3.27	3E-03
AGAP009194	*GSTE2*	glutathione S-transferase epsilon class 2	-2.26	4E-15	-2.02	6E-13
AGAP010004			-2.13	2E-04	-2.81	1E-06
AGAP010367			-2.04	3E-04	-2.70	2E-06
AGAP010794			-2.21	3E-07	-2.71	3E-10
AGAP010854		solute carrier family 45, member 1/2/4	-5.05	1E-03	-3.15	3E-02
AGAP012391		DUF1298 domain-containing protein	-2.20	2E-04	-2.63	5E-06
AGAP012399		maltase	-2.15	6E-07	-2.51	2E-09
AGAP012644			-2.72	6E-06	-3.51	1E-08
AGAP013094		Elongation of very long chain fatty acids protein	-2.62	8E-07	-2.49	2E-06
AGAP013211			-2.32	6E-03	-3.79	6E-05
AGAP013526			-3.31	7E-05	-4.00	7E-05
AGAP028049		Carrier domain-containing protein	-2.21	1E-09	-2.13	3E-09
AGAP028128	*ABCC9*	ATP-binding cassette transporter (ABC transporter) family C member 9	-2.11	1E-09	-2.60	4E-13
AGAP028586			-3.00	6E-09	-3.46	2E-10

997

998 **Table S5.** Downregulated genes in the circulating hemocytes at 4 hr following both

999 GFP-*E. coli* and *S. aureus* infection.

			E. coli vs injury		*S. aureus* vs injury	
Gene ID	**Gene name**	**Gene description (if annotated)**	**Log2Foldchange**	**Adjusted P**	**Log2Foldchange**	**Adjusted P**
AGAP000144		progestin and adipoQ receptor family member 3	-2.48	1E-03	-2.80	2E-04
AGAP001106		Disconnected protein	-2.32	9E-11	-2.77	1E-15
AGAP001476		Innexin inx2	-2.24	1E-09	-2.81	1E-15
AGAP001635		sodium-coupled monocarboxylate transporter 2	-2.53	2E-10	-2.61	3E-11
AGAP002072			-2.08	4E-05	-2.59	2E-07
AGAP002429	*CYP314A1*	cytochrome P450	-2.14	7E-03	-3.53	1E-06
AGAP003494		sugar transporter ERD6-like 7	-2.62	4E-07	-2.68	6E-08
AGAP004954		rhythmically expressed gene 2 protein	-2.09	3E-11	-2.67	3E-18
AGAP005752		glucosyl/glucuronosyl transferases	-2.06	5E-05	-2.50	1E-07
AGAP007990		glucosyl/glucuronosyl transferases	-2.75	2E-02	-3.13	6E-03
AGAP008237		Putative G-protein coupled receptor GPCR	-2.01	2E-07	-3.28	2E-18
AGAP008629		N-acetyltransferase domain-containing protein	-2.01	1E-07	-3.47	8E-16
AGAP009381		Cellular retinaldehyde-binding protein	-2.18	9E-05	-3.37	2E-07
AGAP009382			-4.31	1E-02	-4.17	1E-02
AGAP010794			-2.33	4E-06	-3.53	4E-10
AGAP011714			-2.18	4E-08	-2.28	2E-09
AGAP012216		sterol O-acyltransferase	-2.15	8E-08	-3.36	1E-16
AGAP028204		Alpha-mannosidase	-2.04	1E-02	-2.04	1E-02
AGAP028745			-2.03	4E-03	-2.12	2E-03

1000

1001 **Table S6.** Gene names, gene IDs, and primers used.

Application	Gene	dsRNA	VectorBase ID[a]	Primer sequence (forward and reverse) [b]
qPCR	*Rps7*		AGAP010592	GACGGATCCCAGCTGATAAA
qPCR				GTTCTCTGGGAATTCGAACG
qPCR	*Rps17*		AGAP004887	GACGAAACCACTGCGTAACA
qPCR				TGCTCCAGTGCTGAAACATC
qPCR	*rel2*		AGAP006747	TTCGCTGCTCGACTTTCACT
qPCR				CCAACCGAAGGCAGCAAATC
qPCR	*caspar*		AGAP006473	TCGTAGCCAATGCGAAGTGT
qPCR				TCGTTCGTTCTCTTCACGCA
qPCR	*PGRP-LA-RA*		AGAP005205	GGCAATGGCGGAAATACGAC
qPCR				GGTTCCGCTGAAGGTAGTCC
qPCR	*PGRP-LA-RB*		AGAP005205	GGTACGTTTGACGCGGATC
qPCR				GTCCGCGGTTCTGATTGTT
qPCR	*PGRP-LA-RC*		AGAP005205	GCAATGGCGGAAATACGAC
qPCR				ATGCCCGGCGAAGTATATG
qPCR	*JNK1*		AGAP029555[c]	TGTTTCCGACCGACTCGAA
qPCR				CGTCCACGCTGTGATCGTA
qPCR	*JNK3*		AGAP009460	ACAGTCTTAAGCATCCCGGC
qPCR				GCGGCAAAACACACTCCTTT
qPCR	*puckered*		AGAP004353	ATTCAACGGAGGTCGATTTG
qPCR				AACTTTCTAGCCCCCATCGT
qPCR	*TEP1*		AGAP010815	GACGTCCAAATACGGATCTCA
qPCR				CTTTCAGGCATCACCCGTAT
qPCR	*cec3*		AGAP000694	TTCCCAGTGCATCTGTGTCC
qPCR				GAGCTTTGTAGCCGGCAATG
qPCR	*def1*		AGAP011294	GCAACGATCGTCTGTACCATT
qPCR				GCTTGGCCCGATAGTTCTC
RNAi	*bla(Ap^R)*	ds*bla(Ap^R)*	(Bacterial gene)	TAATACGACTCACTATAGGGCCGAGCGCAGAAGTGGT
RNAi				TAATACGACTCACTATAGGGAACCGGAGCTGAATGAA
RNAi	*rel2*	ds*rel2*	AGAP006747	TAATACGACTCACTATACGGAGAAGTCGAAGAAAACG
RNAi				TAATACGACTCACTATACACAGGCACACCTGATTGAG
RNAi	*caspar*	ds*caspar*	AGAP006473	TAATACGACTCACTATAGGGACAGAAGGCCGCTTT
RNAi				TAATACGACTCACTATAGGGAGTGGTGGTGCAGAGTT
RNAi	*PGRP-LA*	ds*PGRP-LA-RARB* [d]	AGAP005205	TAATACGACTCACTATAGGGAGATACTGTTCGACACCA
RNAi				TAATACGACTCACTATAGGGCTGGCTGTGGTAGGTTT
RNAi	*PGRP-LA*	ds*PGRP-LA-RC*	AGAP005205	TAATACGACTCACTATAGGGCACATGGTCATCGATC
RNAi				TAATACGACTCACTATAGGGATCGATTTTGGGTATTC
RNAi	*JNK1/JNK3*	ds*JNK1/3* [e]	AGAP0290555 /AGAP009460	TAATACGACTCACTATAGGGGTCACGCCTTCTACACCGTC
RNAi				TAATACGACTCACTATAGGGCAGCCCAAAGTCGAGGATT
RNAi	*puc*	ds*puc*	AGAP004353	TAATACGACTCACTATAGGGTGAAACATAAATCGCCCTGC
RNAi				TAATACGACTCACTATAGGGGACAGACCCTTGTAGCGCAT

1002
1003 a Vectorbase IDs were obtained from the AgamP4 assembly in www.vectorbase.org (exception: *bla(Ap^R)*).
1004 b Underlined sequences are specific to the T7 RNA polymerase promoter sites needed for dsRNA synthesis.
1005 c Previous gene ID of JNK1 is AGAP009461.
1006 d ds*PGRP-LA-RARB* targets both the RA and RB splice variants of *PGRP-LA*.
1007 e ds*JNK1/3* targets both *JNK1* and *JNK3*.
1008
1009
1010
1011
1012
1013

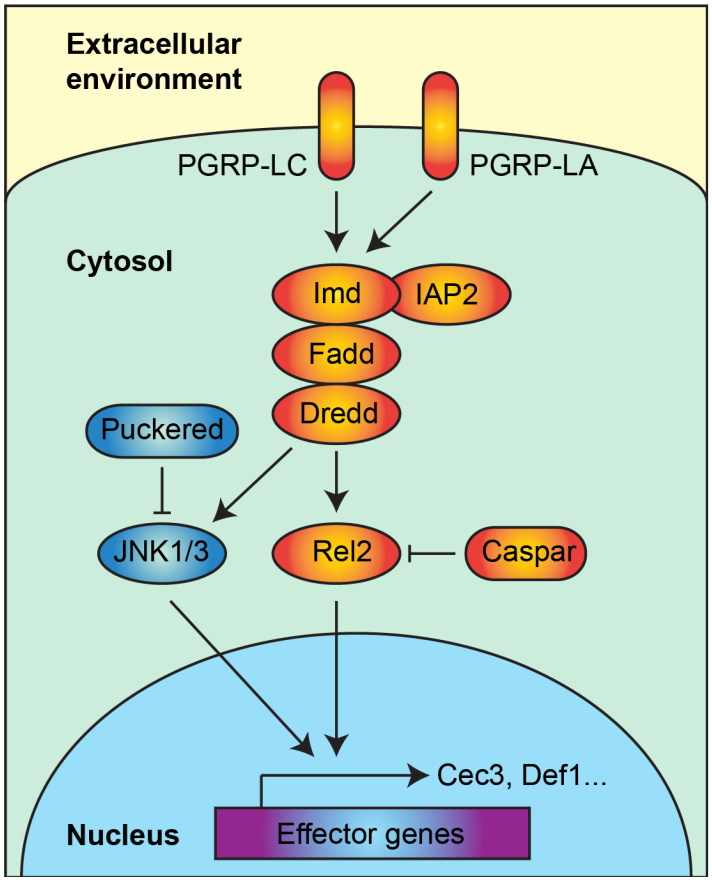

1014
1015
1016 **Figure S1. The IMD and interlinked JNK pathways are two of the major immune**
1017 **pathways in mosquitoes.** The activation of PGRP-LC triggers the IMD signaling
1018 pathway, which includes IAP2, imd, fadd and dredd. This activation dissociates the
1019 transcription factor, rel2, from the inhibitor protein, caspar. Rel2 then translocates into
1020 the nucleus and induces the production of effectors such as cec3 and def1. Although
1021 PGRP-LC is the canonical activator of the IMD pathway, PGRP-LA has also been
1022 implicated as an upstream activator of this immune pathway. The IMD pathway
1023 bifurcates into the JNK pathway, which activates JNK1 and JNK3, and induces the
1024 expression of effector genes. The JNK pathway is negatively regulated by puckered.
1025
1026
1027
1028

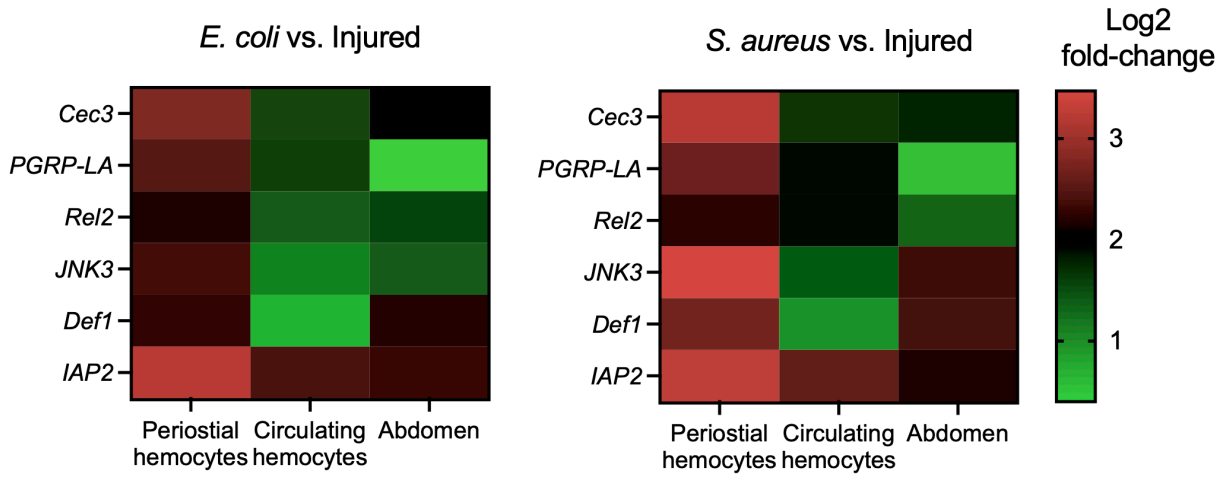

1029
1030
1031 **Figure S2. Infection upregulates IMD and JNK pathway genes more highly in the**
1032 **heart and periostial hemocytes than in the circulating hemocytes or the abdomen.**
1033 Heat maps show that all six IMD and JNK pathway genes identified in our unbiased
1034 screen are more highly upregulated after *E. coli* and *S. aureus* infection in the heart and
1035 periostial hemocytes than in the other tissues.
1036
1037
1038
1039

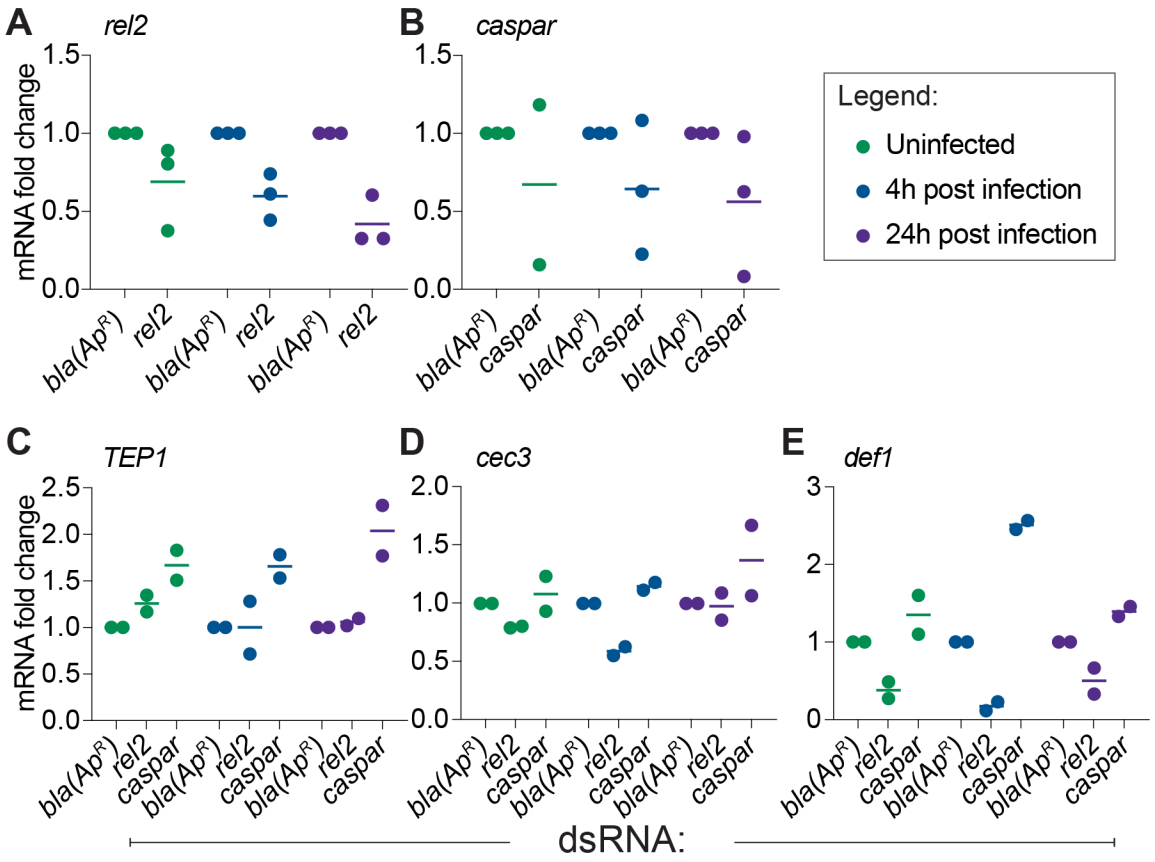

1040
1041
1042 **Figure S3. RNA interference-mediated gene silencing of *rel2* and *caspar* reduces**
1043 **their mRNA abundance while altering the mRNA abundance of *TEP1*, *cec3* and**
1044 ***def1*.** Relative mRNA abundance of *rel2* (A), *caspar* (B), *TEP1* (C), *cec3* (D), and *def1*
1045 (E) in mosquitoes injected ds*bla(Ap^R)*, ds*rel2* or ds*caspar*. mRNA abundance was
1046 measured in mosquitoes that were not infected or had been infected with GFP-*E. coli*
1047 for 4 or 24 hr. Horizontal line, mean; Circles, individual biological trials. Data are relative
1048 to mRNA abundance in the ds*bla(Ap^R)* group of that specific trial and treatment.
1049

1050

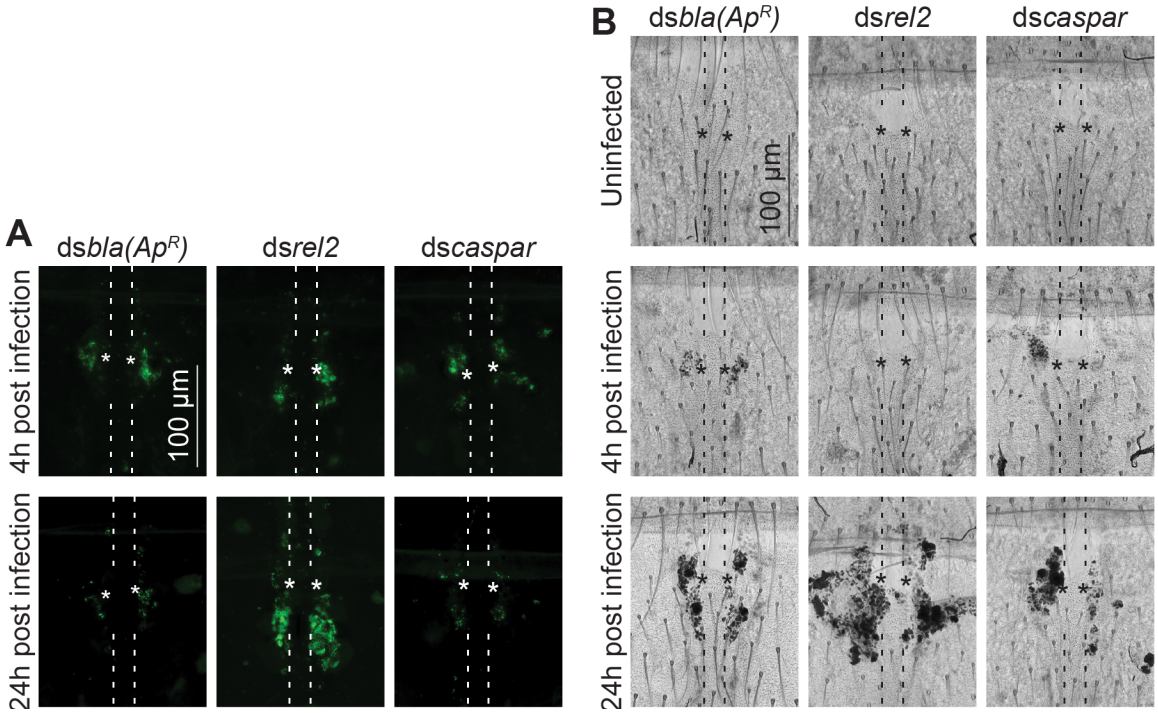

1051
1052
1053 **Figure S4. The IMD pathway affects GFP-*E. coli* and melanin accumulation at the**
1054 **periostial regions.** (*A*) Fluorescence images show the accumulation of GFP-*E. coli*
1055 (green) around a single pair of ostia (asterisks) on a segment of the heart (outlined by
1056 dotted lines) of ds*bla(Ap^R)*, ds*rel2* and ds*caspar* mosquitoes that had been infected with
1057 GFP-*E. coli* for 4 or 24 hr. (*B*) Bright field images show the accumulation of melanin
1058 (dark deposits) around a single pair of ostia (asterisks) on a segment of the heart
1059 (outlined by dotted lines) of ds*bla(Ap^R)*, ds*rel2* and ds*caspar* mosquitoes that were not
1060 infected or had been infected with GFP-*E. coli* for 4 or 24 hr. Anterior is on top.
1061 Quantification of all mosquitoes assayed is presented in figures 3A and 3B.
1062
1063
1064
1065

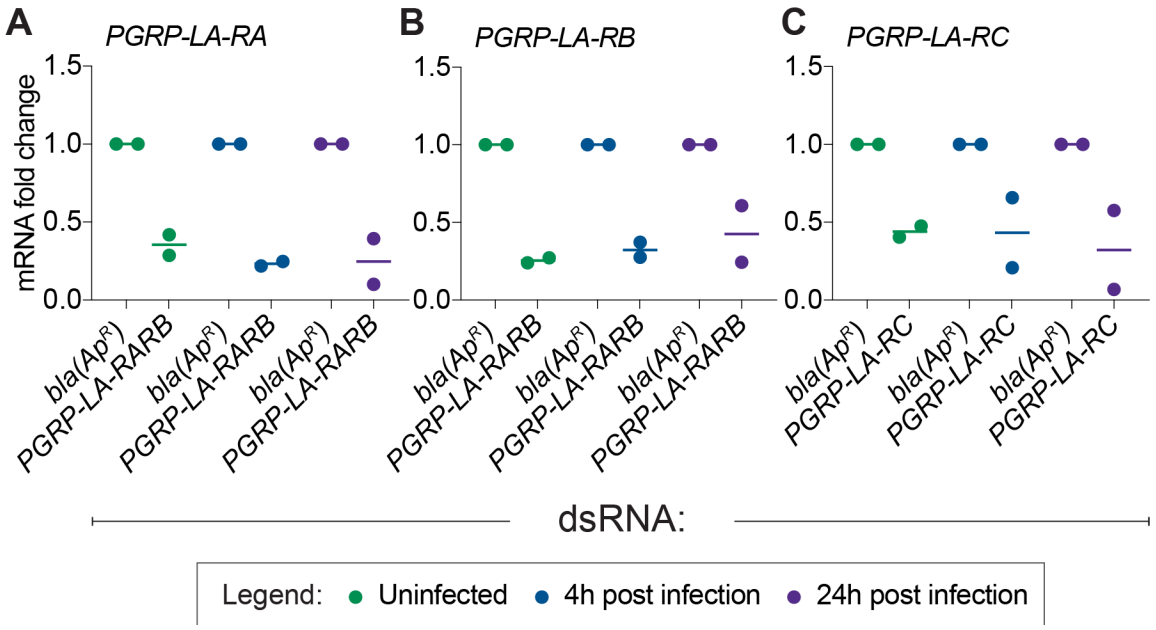

1066
1067
1068 **Figure S5. RNA interference-mediated gene silencing of *PGRP-LA* reduces the**
1069 **mRNA abundance of all splice variants.** Relative mRNA abundance of *PGRP-LA-RA*
1070 (A), *PGRP-LA-RB* (B) and *PGRP-LA-RC* (C) in mosquitoes injected ds*bla(Ap^R)*,
1071 ds*PGRP-LA-RARB* or ds*PGRP-LA-RC*. mRNA abundance was measured in
1072 mosquitoes that were not infected or had been infected with GFP-*E. coli* for 4 or 24 hr.
1073 Horizontal line, mean; Circles, individual biological trials. Data are relative to mRNA
1074 abundance in the ds*bla(Ap^R)* group of that specific trial and treatment.
1075

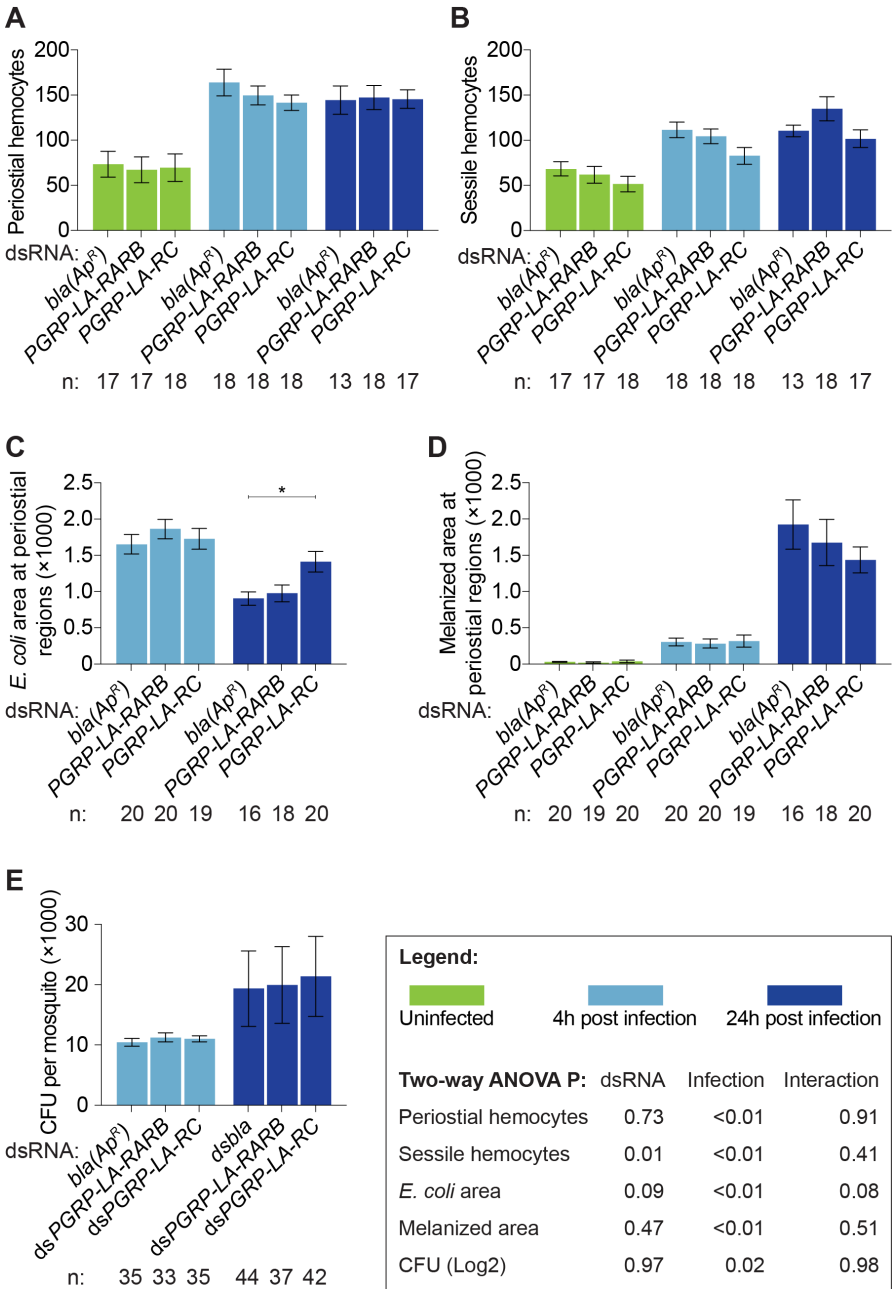

Figure S6. The RC splice form of PGRP-LA regulates phagocytosis by periostial hemocytes. (*A*-*E*) Graphs for ds*bla(Ap^R)*, ds*PGRP-LA-RARB* and ds*PGRP-LA-RC* mosquitoes that were not infected or had been infected with GFP-*E. coli* for 4 or 24 hr. The graphs show: (*A*) average number of periostial hemocytes; (*B*) average number of sessile hemocytes outside of the periostial regions in the tergum of abdominal segments 4 and 5; (*C*) pixel area of GFP-*E. coli* in the periostial regions; (*D*) pixel area of melanin in the periostial regions; and (*E*) the systemic GFP-*E. coli* infection intensity. Graphs show the mean and S.E.M. The data were analyzed by two-way ANOVA (bottom box), followed by Dunnett's multiple comparison test. N indicates sample size. Asterisk in graph indicate post-hoc $p < 0.05$.

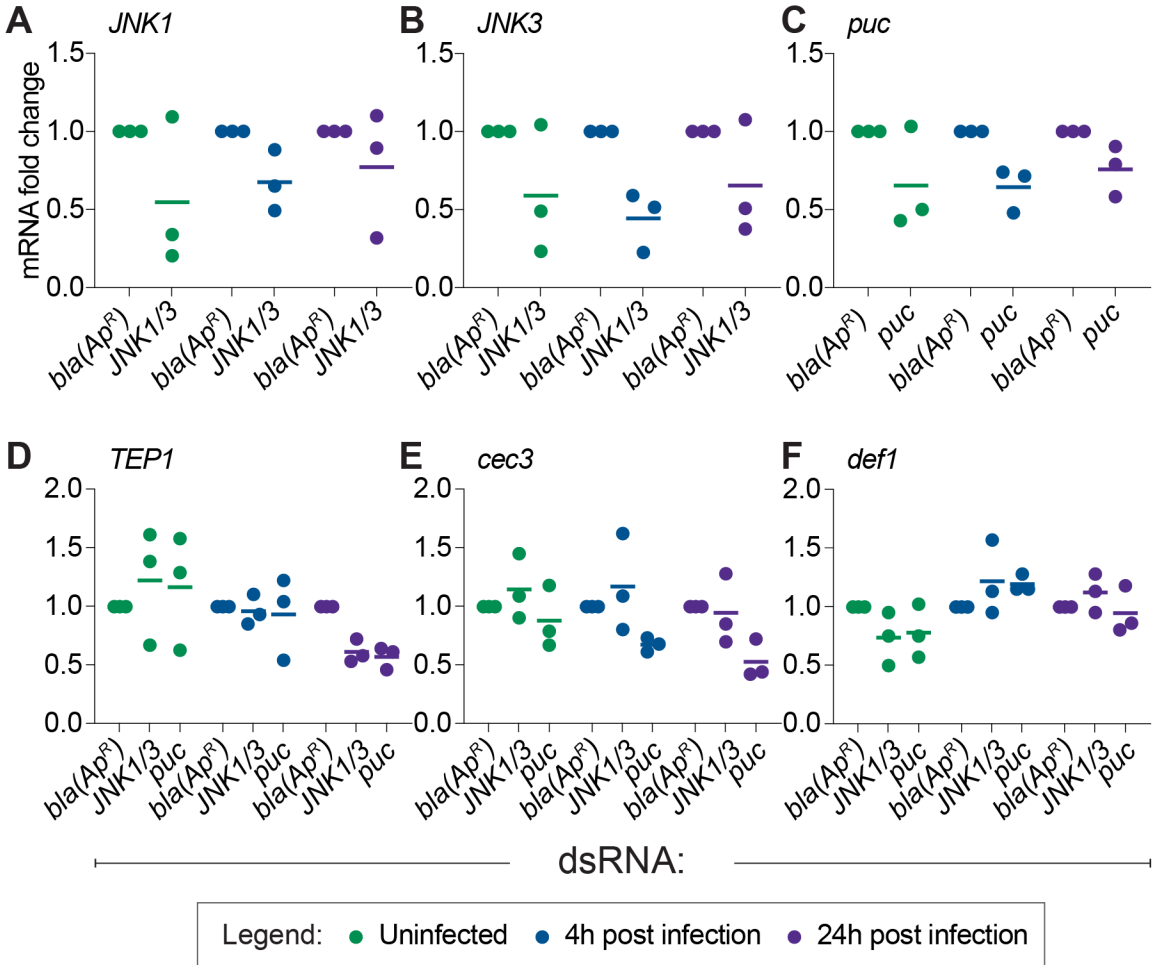

Figure S7. RNA interference-mediated gene silencing of *JNK1*, *JNK3* and *puc* reduces their mRNA abundance while having a limited impact on the mRNA abundance of *TEP1*, *cec3* and *def1*. Relative mRNA abundance of *JNK1* (A), *JNK3* (B), *puc* (C), *TEP1* (D), *cec3* (E), and *def1* (F) in mosquitoes injected ds*bla(Ap^R),* ds*JNK1/3* or ds*puc*. mRNA abundance was measured in mosquitoes that were not infected or had been infected with GFP-*E. coli* for 4 or 24 hr. Horizontal line, mean; Circles, individual biological trials. Data are relative to mRNA abundance in the ds*bla(Ap^R)* group of that specific trial and treatment.

1101

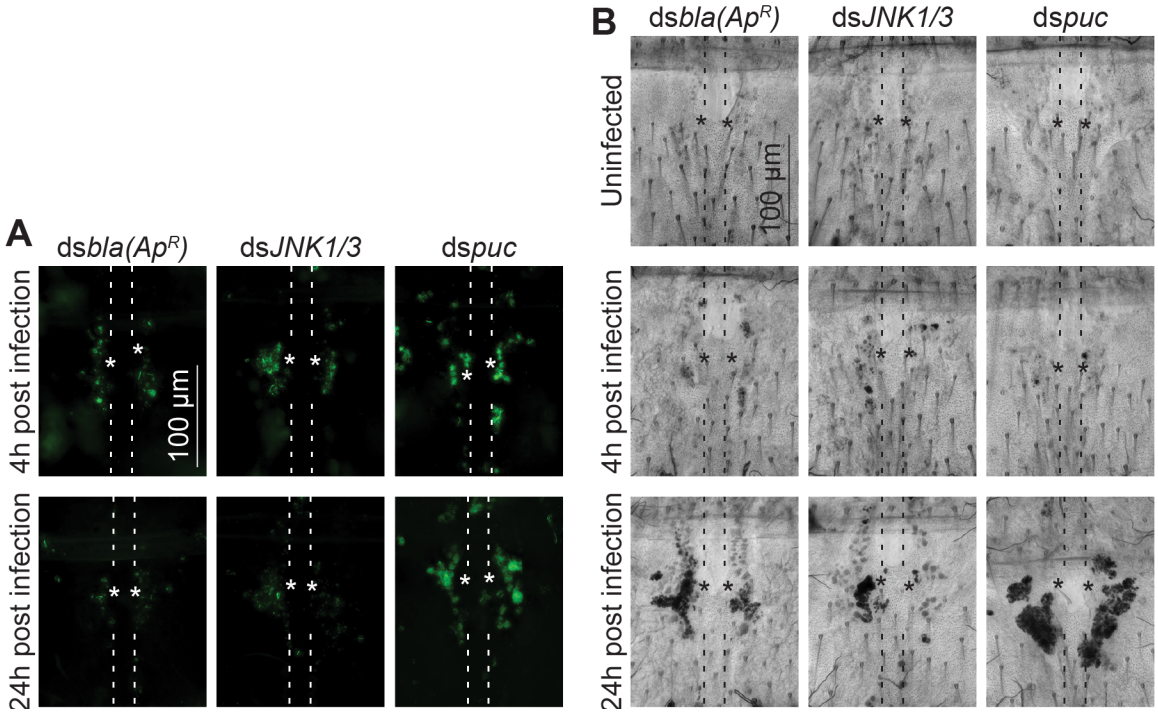

1102
1103
1104 **Figure S8. The JNK pathway affects GFP-*E. coli* and melanin accumulation at**
1105 **periostial regions.** (*A*) Fluorescence images show the accumulation of GFP-*E. coli*
1106 (green) around a single pair of ostia (asterisks) on a segment of the heart (outlined by
1107 dotted lines) of ds*bla(Ap^R)*, ds*JNK1/3* and ds*puc* mosquitoes that had been infected
1108 with GFP-*E. coli* for 4 or 24 hr. (*B*) Bright field images show the accumulation of melanin
1109 (dark deposits) around a single pair of ostia (asterisks) on a segment of the heart
1110 (outlined by dotted lines) of ds*bla(Ap^R)*, ds*JNK1/3* and ds*puc* mosquitoes that were not
1111 infected or had been infected with GFP-*E. coli* for 4 or 24 hr. Anterior is on top.
1112 Quantification of all mosquitoes assayed is presented in figures 5A and 5B.
1113
1114